Elevation for a humanoid robot

Victor Oldensand

Degree in Mechanical Engineering
Bachelor Thesis

February 10th - June 13th 2025

Academic supervisor:
Maria Makarov
maria.makarov@centralesupelec.fr

Company supervisor:
Matthieu Lapeyre
matthieu.lapeyre@pollen-robotics.com

CentraleSupélec | université PARIS-SACLAY

Abstract

For a humanoid robot to effectively operate in human environments, it must be able to interact with objects located on both elevated surfaces and at ground level—such as picking up a tool from a table or retrieving an item from the floor. The Reachy robot from Pollen Robotics, however, currently has limitations in vertical mobility that constrain this capability. This report investigates the design of an elevation mechanism for the Reachy 2 humanoid platform to enable automatic vertical adjustment. It begins with an exploration of potential mechanisms suited to the existing design and human-inspired kinematics. From this, one mechanism is selected for in-depth analysis based on engineering criteria such as cost, weight, and repairability. The goal is to support the development of a more versatile and adaptable humanoid robot capable of performing tasks across a greater range of environments and applications.

Résumé

Pour qu'un robot humanoïde fonctionne efficacement dans un environnement conçu pour les humains, il doit pouvoir interagir avec des objets situés à la fois sur des surfaces surélevées et au niveau du sol, comme saisir un outil sur une table ou ramasser un objet tombé au sol. Le robot Reachy développé par Pollen Robotics présente actuellement des limitations de mobilité verticale qui restreignent cette capacité. Ce rapport étudie la conception d'un mécanisme d'élévation pour la plateforme humanoïde Reachy 2, afin de permettre un ajustement vertical automatique. Il commence par une exploration de plusieurs mécanismes compatibles avec la conception existante et la cinématique inspirée de l'anatomie humaine. Ensuite, un mécanisme est sélectionné pour une analyse approfondie en fonction de critères techniques tels que le coût, le poids et la réparabilité. L'objectif est de contribuer au développement d'un robot humanoïde plus adaptable, capable d'effectuer des tâches dans une plus grande variété d'environnements et d'applications.

CentraleSupélec | université PARIS-SACLAY

Acknowledgements

I would like to thank Matthieu Lapeyre from Pollen Robotics for his support and for making this thesis a possibility. I hope this work will offer insights for the Pollen Robotics team to provide the next generation of the Reachy robot with the legs to stand on. In addition, I am thankful for the support from Augustin Crampette, Jeremy Laville, Étienne Besancon, and Miguel Rodrigues from Pollen Robotics, who provided technical assistance during the analysis in the study. Last, thanks to my project supervisor at CentraleSupélec, Maria Makarov, for sharing her invaluable insight into this project's design and evaluation process.

Paris, June 2025
Victor M. Oldensand

Glossary

Bang-Bang A trapezoidal motion profile that consists of an acceleration phase, constant velocity phase, and deceleration phase, creating a characteristic trapezoid-shaped velocity curve over time. 13, 14

Chain typology The categorization of mechanical linkage systems based on their structural characteristics. It provides a systematic way to describe how joints and links are connected in mechanical systems. 29

Denavit-Hartenberg The Denavit-Hartenberg (D-H) convention is a standardized approach for describing the kinematic structure of serial robotic manipulators. This allows for the systematic derivation of transformation matrices between adjacent joints in a kinematic chain. 30, 36

DoF For a rigid body (eg. end-effector), the degree of freedom (DoF) is the minimum number of coordinate values required to represent its pose in space. For a robot, it is the minimum number of values required to represent its pose configuration (i.e. number of actuated joints). 6, 15, 16, 20, 22, 25, 26, 30, 44

Holonomic A mobile robot platform that can move instantaneously in any direction in its plane of motion without needing to rotate first. 6–8, 25–27, 39

PR Pollen Robotics (PR) is the client company for this thesis. Owned by Hugging Face, it is an open-source robotics company that builds robotic hardware platforms and software development kits for research purposes. Its main product is Reachy, a semi-humanoid robot with articulated arms and head on a holonomic base. 7, 9, 10, 13–15, 17–19, 24, 25, 27, 28, 43

Transformation matrix A mathematical tool used to perform coordinate transformations in robotics. It encodes both rotation and translation operations in a single matrix, allowing spatial transformations to be expressed as matrix multiplications. 30, 36

Workspace The complete set of points that a robot's end-effector can reach in three-dimensional space. 6, 10–12

Contents

1 Introduction

Humanoid robotics has advanced rapidly over the last decade due to the convergence of several technical developments. These include improvements to high-torque and high-precision actuators, multimodal generative AI, and exteroceptive devices such as cameras and sensors (Diamandis, 2024). Open-source robotics companies have built hardware platforms that take advantage of these improvements to lower the barriers to entry for researchers, developers, and companies to build advanced features on-top of existing work. For example, humanoids such as the H1 robot from Unitree are systems with kinematics similar to that of humans. Significant research efforts are focused on improving these platforms to the extent where their agility and dexterity inch closer to - or beyond - that of humans (Fu et al., 2024).

The term humanoid is not well-defined, as varieties of the concept exist to improve the capabilities of the robot in certain environments - such as wheel-legged humanoids in factories. In such cases, alternative mechanisms are designed to emulate the key DoFs that human legs and feet typically provide. For wheel-legged and holonomic humanoids, one of the key challenges is enhancing their ability to interact with objects across a wide range of positions. Increasing the DoFs—particularly in the legs and arms—expands the robot's workspace and improves its capacity to manipulate objects at different heights and angles. For example, a humanoid robot with a fixed torso may struggle to pick up objects from both the ground and elevated surfaces without repositioning its entire body. By integrating an elevation mechanism, the robot is able to extend or retract its reach dynamically. This enhances not only its functional versatility but also its efficiency in human-robot collaboration, industrial applications, and assistive robotics (Bjelonic et al., 2023).

This report explores the development of an elevation mechanism for the Reachy platform by Pollen Robotics, focusing on practical engineering considerations and potential solutions.

1.1 Case background

Pollen Robotics is an open-source robotics company that develops a humanoid hardware platform called Reachy. The latest version, Reachy 2, has two 7 DoFs robotic arms, a parallel neck mechanism, and a holonomic mobile platform. The intention is for the robot to act as a stable AI-ready hardware platform for human-robot interaction with advanced manipulation and teleoperation abilities (Pollen Robotics, 2025a). The company sees the robot as an adaptable platform for research and development applications.

Figure 1 illustrates the Reachy 2 hardware with its humanoid torso and holonomic base. Currently, the robots legs must be manually adjusted by a human operator for elevation. The company aims to enhance Reachy with the ability to autonomously adapt its height to interact with objects on various levels of elevation, including the ground.

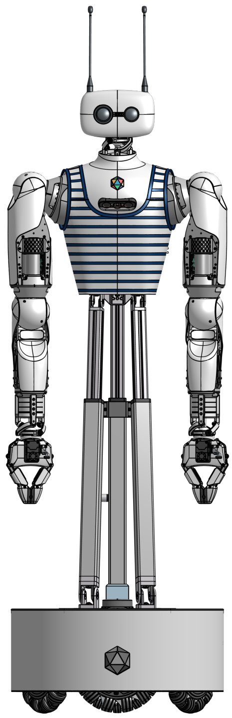

Figure 1: Reachy 2 hardware platform (Pollen Robotics, 2025c)

Currently, the torso is fixed to a platform via three linear clamp rails that are adjusted after rotating three levers. In 2024, Alexis Raynaud, an intern at Pollen Robotics, conducted a preliminary study on the potential of using an automated Stewart platform to replace this (Raynaud, 2024). However, after various discussions with the team at Pollen Robotics (PR), I understood that the choice of link architecture for the elevation system is largely undecided. Consequently, this report is divided into two stages: an explorative study of alternative mechanisms, and a deeper study of one selected mechanism.

1.2 Purpose statement

This report aims to offer insights into hardware development analysis for an open-source robotics company, particularly for Pollen Robotics' Reachy 2. In addition, I provide an overview of elevation mechanisms for wheel-legged, holonomic, and bipedal robots. Furthermore, this report aims to present practical engineering considerations used for analysis and selection, such as weight, cost, repairability, and portability. Hopefully these insights can support future work in robotic mechanisms.

1.3 Research question

How can an elevation link mechanism be designed and analyzed to enable automatic vertical adjustment to the ground and to elevated surfaces for the Reachy humanoid robot?

1.4 Delimitations

This thesis focuses exclusively on the design and analysis of elevation mechanisms for the Reachy 2 robot. Thus, the findings may not generalize to other open-source robots due to differences in design, actuators, and purposes. In addition, the technical implementation and evaluation of the mechanism is limited due to time and resource constraints. Subsequently, the report does not include research or prototyping beyond the digital twins of the robot, i.e. CAD modeling and theoretical analysis. The focus lies on the kinematics and dynamics of the mechanisms. I also refrain from making assumptions about the remaining parts of the next Reachy robot, meaning I design around the current torso.

2 Problem description

In this section I define the problem space and its mathematical formulation. This clarifies the eventual design targets for both the comparative- and the detailed analysis of Section 5 and 7, respectively.

2.1 System's geometric description

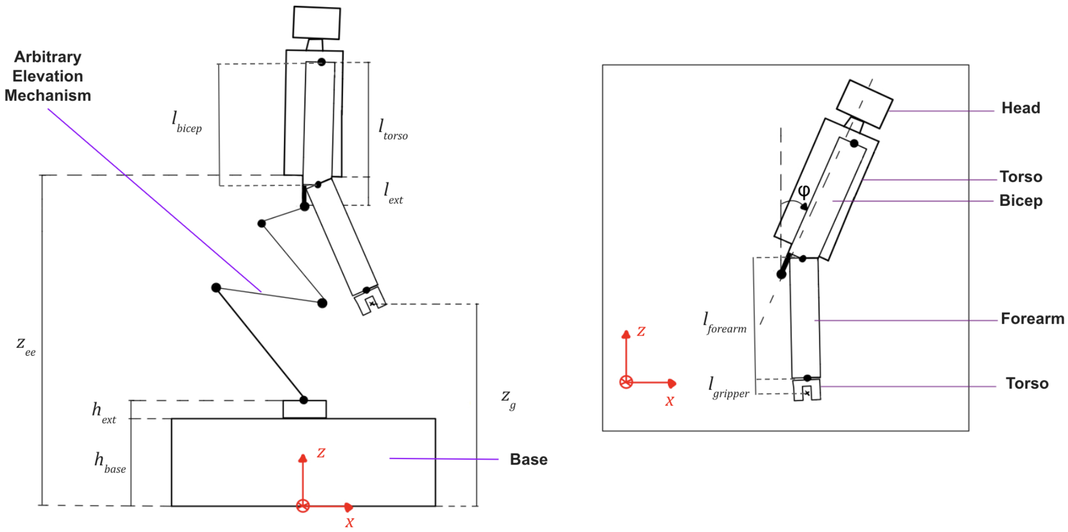

Figure 2: Side-view of the problem with an arbitrary mechanism (not to scale)

The sketches in Figure 2 illustrate the key values that define the problem space such as the current height of the Reachy torso base, z_{ee}, the current height of the gripper, z_g, and the pitch, ϕ. Note that the end-effector position is defined at the midpoint of the mechanical gripper as per PRs specifications (Pollen Robotics, 2025b). Additionally, I define the base of Reachy's torso as the end-effector (ee) of the elevation mechanism, so I subscript its values with *ee*. I also define several constants such as $h_{base} = 240.1\,\text{mm}$, $l_{bicep} = 280\,\text{mm}$, $l_{forearm} = 280\,\text{mm}$, $l_{gripper} = 110\,\text{mm}$, and $l_{torso} = 245\,\text{mm}$. Finally, the design values l_{ext} and h_{ext} specify how far the pitch pivot point extends beyond the torso and the height above the base on which the elevation mechanism begins, respectively.

2.2 Vertical stroke

The maximum height that the base of Reachy 2's torso can reach under the current manual mechanism is $z^*_{ee,max} = 970.1\,\text{mm}$. In the scope of this report, I assume that Reachy's maximum height remains unchanged.

To determine the desired minimum height, I set a condition requiring Reachy's minimum attainable workspace radius at ground level, r_{target}, when $\theta = 0°$ to match $0.3\,\text{m}$, as decided with help from PR engineers. The area this encompasses can be calculated using Equation 1 as follows:

$$A = 2\pi r^2 - 2r^2\left(\zeta - \frac{1}{2}sin(2\zeta)\right) \tag{1}$$

where $\zeta = \arccos(d_{\text{shoulder}}/r_{\text{target}})$ and $d_{\text{shoulder}} = 200\,\text{mm}$. This equates to $A_{\text{target}} = 0.5035\,\text{m}^2$. As the limit of Reachy's reach is determined by the contour lines traced by its straight arm on the ground, I can extract a $z_{ee,min}$ as a function of the desired ground workspace, A, and ϕ. I present a simple scalar optimization problem:

$$z_{ee,min} = \underset{z_{ee}\in[z_{\text{min}},z_{\text{max}}]}{\text{argmin}} \left|A(z_{ee},\phi) - A_{\text{target}}\right| \tag{2}$$

Where $z_{\text{min}} = h_{\text{base}}$ and $z_{\text{max}} = l_{\text{arm}} - l_{\text{torso}}$ refer to the constraints on the lowest and highest accepted values. We illustrate the mathematical formulation in Figure 3.

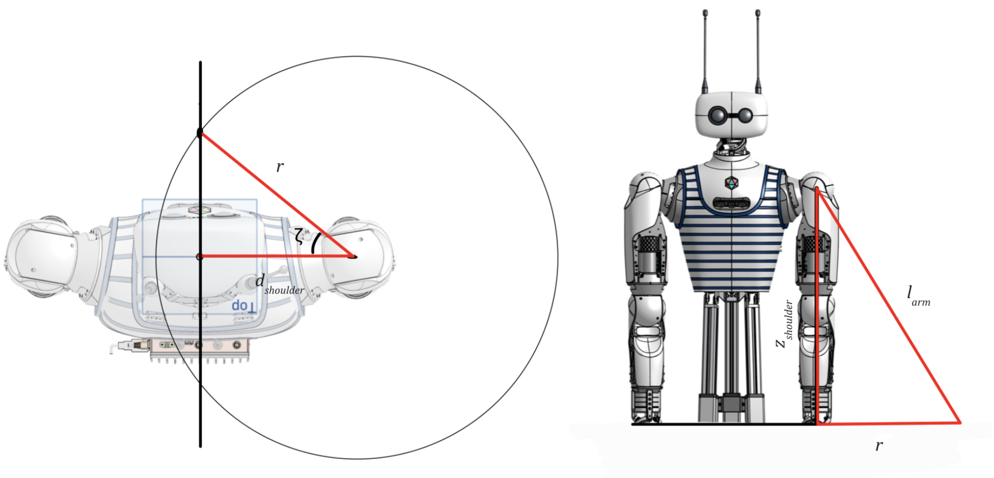

Figure 3: Top (left) and front (right) view of the $z_{ee,min}$ problem (not to scale).

To determine the radius of the ground workspace per arm for a pitch of $\theta = 0°$ we use Equation 3 as follows:

$$r = \sqrt{l_{\text{arm}}^2 - z_{\text{shoulder}}^2} \tag{3}$$

where $l_{\text{arm}} = l_{\text{bicep}} + l_{\text{forearm}} + l_{\text{gripper}}$ and $z_{\text{shoulder}} = z_{ee} + l_{\text{torso}}$. Consequently, for a target ground workspace of $0.5035\,\text{m}^2$, I calculate $z_{ee,min} = 354.1\,\text{mm}$, as illustrated in Figure 4. Finally, the total vertical stroke should, thus, be $\Delta z_{ee} = z_{ee,max} - z_{ee,min} = 616\,\text{mm}$.

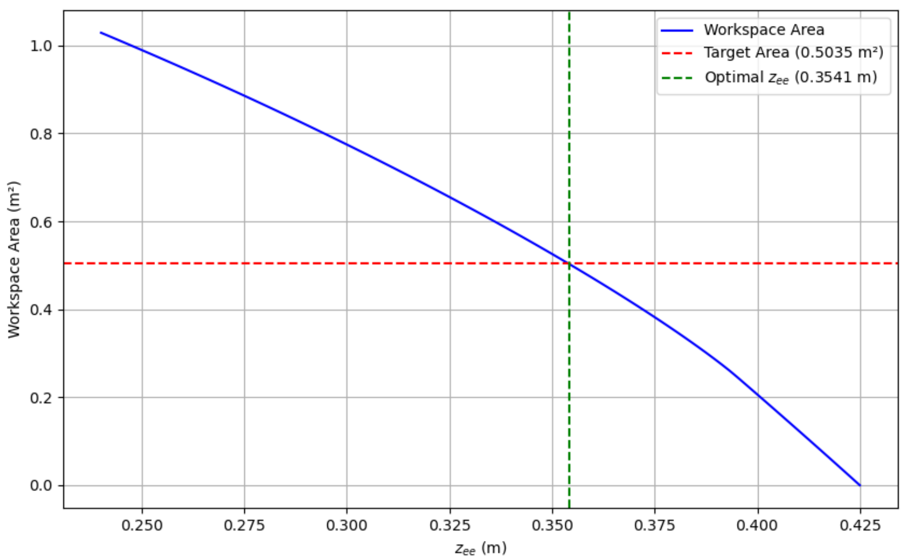

Figure 4: Plot of z_{ee} values against resulting workspace area $A(z_{ee})$.

2.3 Pitch range

The intention behind providing Reachy with pitch at the base of the torso (other than center of mass control), is to increase the size of its achievable workspace on the floor. The reduction in height of the shoulders of Reachy as a function of the pitch angle is:

$$\Delta z_{\text{pitch}} = (l_{\text{torso}} + l_{\text{ext}})(1 - cos\theta)$$

The pitch is illustrated in Figure 2. Assuming an extention to the torso of $l_{\text{ext}} = 50\,\text{mm}$ I extract the following reductions in $z_{shoulder}$ as a function of the pitch.

$\theta(°)$	Δz_{pitch} @50 (mm)
15	10.05
30	39.52
45	86.40
60	147.50

Table 1: Depth advantage at various pitches

By modifying the pitch in this manner I can visualize the workspace of the robot, as illustrated in Figure 5. At a ±30° pitch, the robot is able to reach 0.5512 m in front, positive x, and ±0.5684 m to the left and right, y-axis. In this report I set ±30° as the maximum pitch.

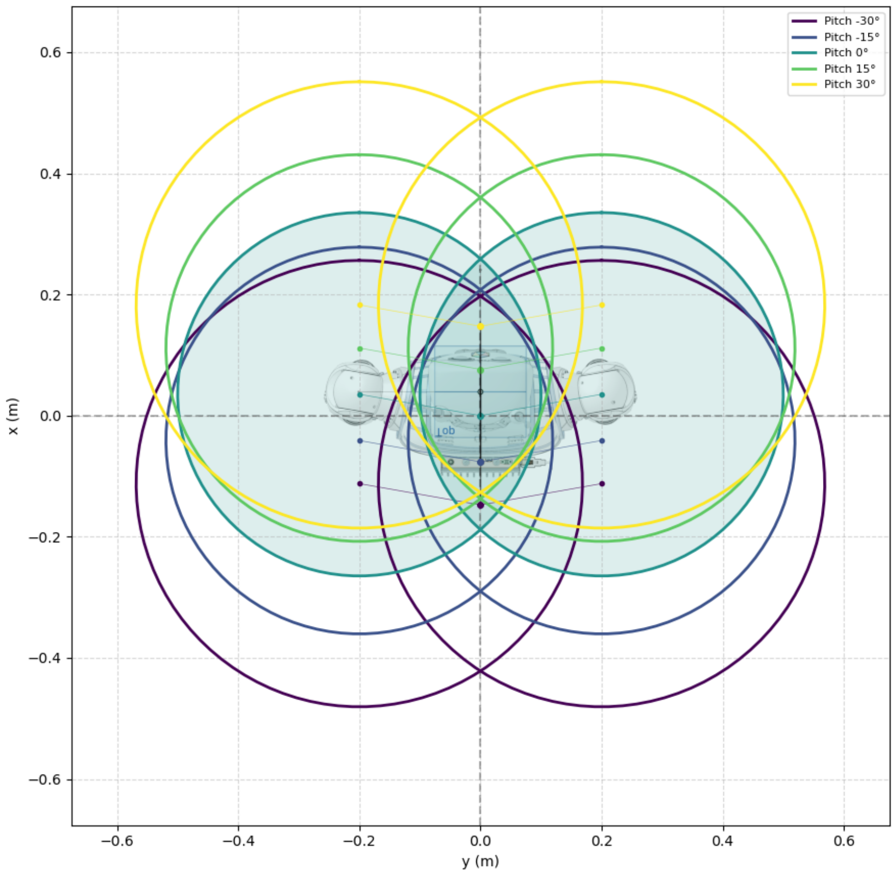

Figure 5: Floor workspace for Reachy at various pitches

2.4 Maximum payload

Discussions with PR engineers during the project made it clear that any elevation mechanism should be capable of supporting a weight of 400 N (i.e. $m_{max} = 40.77$ kg). This takes into consideration the weight of Reachy's upper body, any external objects it interacts with, and a margin of error.

2.5 Motion profile

This section defines the desired motion profile for the elevation mechanism's end effector. To simplify the analysis at this early stage, I constrain the motion to be strictly vertical, whilst allowing for pitch movements only when not elevating. This means that the end effector's elevation motion is described by $\mathbf{x_{ee}(t)} = (x_{ee}, z_{ee}, \phi_{ee}) = (0, z_{ee}, 0)\ \forall\ t$. Furthermore, the PR engineers stated a maximal target of 10 seconds for the elevation system to cover a full stroke. To satisfy this target given a $\Delta z_{ee} = 616$ mm, the average velocity across the motion must be $\dot{z}_{ee} = 61.6$ mm/s. As there are no predefined acceleration or maximum velocity requirements, I use the bang-bang (trapezoidal) motion profile to achieve minimum-time motion under some velocity and acceleration constraints (Grossard, 2025). This is characterized by the phases in Figure 6.

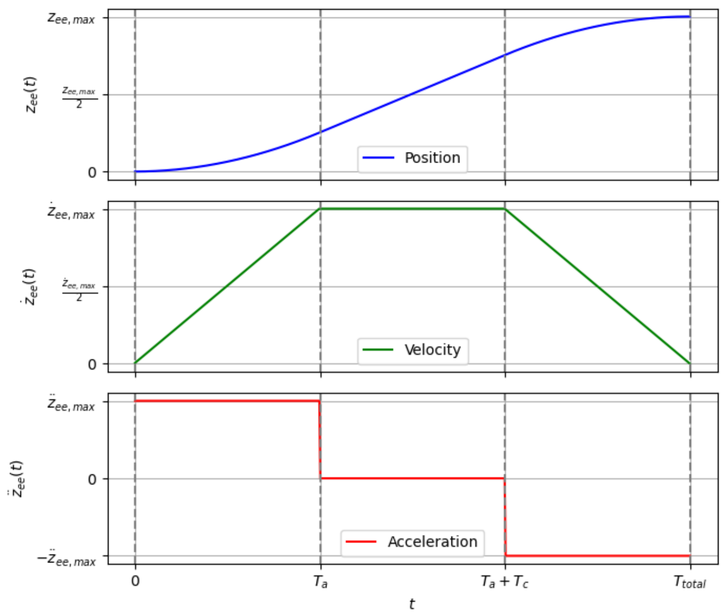

Figure 6: Bang-bang motion profile

To start, I already have the constraints $z_{ee}(0) = z_{ee,min} = 354.1\,\text{mm}$, and $z_{ee}(10) = z_{ee,max} = 970.1\,\text{mm}$. The next step is to define v_{max} and a_{max}, two parameters of the profile. To reduce the required acceleration, I set $v_{max} = 0.1\,\text{m/s}$, which is slightly higher than the expected average elevation speed. In the bang-bang motion profile, a system will be able to reach this velocity before decelerating if $a_{max} > v_{max}^2/\Delta z_{ee} = 0.1^2/0.616 = 0.016\,\text{m/s}^2$. Thus, I set $a_{max} = 0.025\,\text{m/s}^2$ in order to have a margin of error and simplify calculations. With this, the acceleration and deceleration phase of the profile lasts for $T_a = v_{max}/a_{max} = 4\,\text{s}$ each, leading to a constant velocity phase for $T_v = 10 - 2T_a = 2\,\text{s}$.

It is, however, important to mention that these parameters are free to select differently. If PR desires to reduce the stroke time to eg. 5 seconds, the corresponding v_{max} and a_{max} can be chosen accordingly.

2.6 Target specifications

To summarize the results of Section 2.1 to 2.5, I provide all the key motion specifications in Table 2.

Target specification	**Value**
Vertical stroke (Δz_{ee})	616.00 mm
Max elevation ($z_{ee,max}$)	970.10 mm
Min elevation ($z_{ee,min}$)	354.10 mm
Pitch (ϕ) range	±30°
Payload (m)	40.77 kg
Average velocity ($\bar{\dot{z}}_{ee}$)	61.6 mm/s
Max velocity ($\dot{z}_{ee,max}$)	100 mm/s
Max acceleration ($\ddot{z}_{ee,max}$)	25 mm/s^2

Table 2: Key design targets

3 Methodology

As a specific architecture for the elevation mechanism was not yet determined by PR, I followed a breadth-first methodology, from criteria identification to detailed analysis.

3.1 Research design

Figure 7 illustrates the four main stages of this study; problem definition, literature review, comparative analysis, and detailed analysis. Prior to secondary research, the first month was spent defining the underlying intention behind an elevation mechanism for Reachy, reviewing Pollen Robotics' past studies, particularly the study by Alexis Reynaud, and determining and ranking the 13 key criteria for the mechanism together with the engineers (Raynaud, 2024). This helped create a common understanding of the goals that the project intended to achieve and its delimitations. For example, by agreeing that the robots pitch and vertical translation were the most important, I could focus the review and analysis on mechanisms that afford one or both of these DoFs.

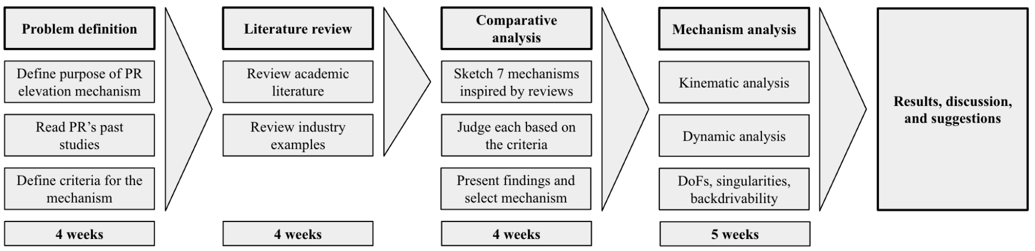

Figure 7: Overview of the research process

Once the problem was clearly defined, I conducted both a literature- and an industry review to cover and compare a broad range of available mechanisms for Reachy's elevation. In total, the review explored the current state-of-the-art robotic elevation and pitch/roll mechanisms while paying particular attention to the criteria defined with Pollen Robotics. The academic review used a scoping method, in which a systematic approach to finding literature is combined with advice from domain experts, using the research question as a starting point. This allowed me to iteratively receive feedback from the PR engineers to redesign my search strategy. To find the relevant literature I used IEEE Xplore, Scopus, and Google Scholar, as they provide the majority of technical publications in the field of robotics (IEEE, 2025; Elsevier, 2025; Google, 2025). However, due to the developing nature of this field, I decided to explore examples from industry by reviewing solutions outside of academia like patents databases, product releases, social media posts by prominent robotics companies, and industry experts. This was also guided by suggestions from PR engineers, my academic supervisor, and a referential approach within the found sources.

From this review, I selected seven architectures for further analysis based on the feasibility of them reasonably integrating with the Reachy platform under the constraint of not modifying the torso. For each architecture, I designed a simplified model in OnShape consisting of only links and joints (PTC Inc., 2025). Simplifications were intentional at this stage as the overarching goal was to compare the kinematic motions each architecture afforded based on the criteria and to visualize these for better interpretation by the PR engineers. Prior to the presentation of findings to PR, each mechanism was graded on a scale of 1-5 (5 = agreement with required property) along the 13 weighted criteria in a Pugh matrix. This provided a preliminary ranking that I could compare with the selection by the PR engineers to determine if our rankings aligned.

The final stage of the study involved a more detailed kinematic and dynamic analysis of the selected mechanism. With a highly parameterized model of the architecture written in Python, I could define a generic version of the architecture that accurately describes its kinematics to provide answers on its afforded DoFs, the achievable workspace of the robot, singularities, and the required torques at each joint. This allows for a debate on gravity compensation and actuator selection, which is discussed at the end of this report.

3.2 Literature & industry review

The academic component of the review followed a *scoping review* methodology, which is suited for emerging technologies where a broad mapping of concepts and approaches is required. Search queries were designed around core themes including "pitch/roll actuation," "humanoid kinematics," and "robotic height adjustment."

To address gaps in academic literature, I also conducted an industry-focused benchmark, including reviews of patents, product documentation, public releases, and online technical content from companies such as Boston Dynamics, Agility Robotics, and Linak.

3.3 Comparative analysis

Inspired by the findings in the literature and industry review, I designed seven potential architectures for the comparative analysis. Each architecture was designed together with a mockup of Reachy's torso in OnShape for better interpretation. By assigning joint restrictions I could also visualize the mechanisms movement via animations. As the designs focused on the motion profiles rather than assembly and manufacturing, they only consisted of joints and simple link structures. This meant that the criteria and evaluation methods used in the comparative analysis needed assumptions to be made about the mechanisms.

Criteria selection

Together with the engineers at PR, I devised 13 criteria that would be used to evaluate each of the 7 architectures. Prior to the evaluation, I held a meeting with two mechanical engineers at PR asking them to rank each criterion based on the level of importance; very important, important, and less important. This allowed me to set a weight between 1 and 3 for each criterion such that the most important criteria would have a greater impact on the overall score for each architecture. It is, however, worth noting that the rank scoring may not be linear (as suggested by my scoring), which should allow for nuance in the architecture selection stage through discussion with the engineers.

#	Criteria	Weight (1-3)	Type	Calc (Y/N)
1	Integration with Reachy 2	3	Pragmatic	N
2	Static load capacity	3	Mechanical	Y
3	Adjustment range	3	Mechanical	Y
4	Actuation speed	2	Mechanical	Y
5	Pitch & roll abilities	1	Pragmatic	N
6	Robustness	3	Heuristic	N
7	Sound level	1	Heuristic	N
8	Weight	2	Heuristic	Y
9	Portability	2	Heuristic	N
10	Parallel mechanism	1	Heuristic	N
11	Repairability	3	Heuristic	N
12	Cost	2	Heuristic	Y
13	Pollen spirit	1	Esthetic	N

Table 3: Evaluation criteria with weights

Table 3 describes the 13 evaluation criteria used in the comparative analysis of elevation architectures. Each criterion is defined in Appendix 10.1.

Evaluation

The criteria are categorized by type; pragmatic, mechanical, heuristic, and esthetic. This is how I define each:

- **Pragmatic**: the criterion is based on best-practice and experience. It is evaluated based on consultations with the PR engineers.
- **Mechanical**: the criterion is physically grounded and distinguishable by architecture and not detail. It is evaluated based on simple calculations used to distinguish mechanisms at an early stage.
- **Heuristic**: the criterion is related to industry expectations and best practices. It is evaluated using a research-backed set of factors to help with scoring. These are tabulated in Appendix 10.3.
- **Esthetic**: the criterion relates purely to the visual design of the mechanism. It is evaluated using feedback from PR engineers combined with the design ethos defined in PR's vision.

The calculations are provided in Appendix 10.2 and the heuristic tables are provided in Appendix 10.3. I scored each mechanism from 1 to 5 on the 13 weighted criteria and listed them in a Pugh matrix. These results were then visualized in network diagrams and descriptive mechanism cards were shared with the PR team prior to our interim meeting. Together, we selected one mechanism for further analysis.

3.4 Detailed analysis

After the review and interim presentation to PR, I selected the Folding mechanism, as described in detail in Section 5, to be analyzed in greater detail. This analytical process began with a 2D sketch of the mechanism, focusing exclusively on pitch and vertical translation—the two primary motions required. I decided to investigate two three part mechanisms that encapsulate the same motion profile: a simple open tree structure and a complex closed chain structure.

Subsequently, I analyzed the kinematics of the simple open tree version to determine the position, velocity, force, and torque at each joint over the course of the elevation motion profile described in Section 2. This helped me determine the achievable workspace of the simple mechanism, which is critical given the requirement that the robot can interact with both elevated objects and the ground. Furthermore, I identified singularities via Jacobian-based analysis. These are critical points where the mechanism may experience undesirable behavior such as large joint velocities.

With knowledge of the simple chain kinematics and dynamics, I could parametrize the complex closed chain structure to match the workspace requirements while sharing the torque at several joints. Visualizing the movement of this parametrized complex model also served as inspiration for actuation and component designs. This provides the PR team with quantitative data necessary for selecting actuators, sizing power supplies, and optimizing motion profiles. Finally, I discuss the possibility of implementing gravity compensation.

4 Literature review

The field of robotic elevation mechanisms is driven by a combination of academic research efforts and industry competition. To reflect these parallel developments, I have structured the literature review to separately examine the academic contributions and industry advancements.

4.1 Academic literature

The applications of robots that employ elevation mechanisms are broad, meaning the efficacy of an architecture is highly dependent on its use-case. While all of the mechanisms studied in the literature review are capable of providing a vertical translation on the load, they vary in the actuation speed, the range, the capacity, and the additional DoFs they afford to the load. Furthermore, the link chains used in each design significantly impact the working volume of the mechanism. In this review, I separate the analysis based on the two overarching kinematic chain structures; serial and parallel mechanisms.

Serial mechanisms

Serial elevation mechanisms are commonly used in academic research projects due to the biomimetic nature of serial link structures. A popular architecture in academia is a three-link anthropomorphic structure, with the links representing the thigh, shank, and foot of the robot. Often, designers of such mechanisms employ pantograph structures and leaf springs to gain mechanical advantage, and to store and release energy during the gait cycle. Some examples include Cassie, which was inspired by the cassowary, KenkenII, and the architecture in Wang et al. (Reher et al., 2019; Hyon et al., 2002, Wang et al., 2024). The KenkenII mechanism uses two hydraulic actuators at the hips as muscles and a tensile spring as a tendon between the knee and ankle joint. The leg proposed by Wang et al. incorporates a two- compliant design based on a pantograph structure, also with embedded leaf springs, aiming to simplify actuation and avoid antagonistic motor work; however, it does not demonstrate a clear improvement in energy efficiency over simpler two-link leg architectures. Similarly, ATRIAS uses a lightweight four-bar leg linkage with embedded fiberglass leaf springs to approximate the spring-mass model dynamics, prioritizing energy-efficient locomotion (Hubicki et al., 2016). However, these mechanisms are designed for robots with bipedal gait or monopedal hopping. As the main subsystems of these mechanisms are not designed for wheeled robots, they should only be used as inspiration in cases like Reachy.

(a) Cassie (Reher et al., 2019)

(b) BHR-W (Lingxuan et al., 2021)

(c) Ascento (Klemm et al., 2019)

Figure 8: Examples of serial elevation mechanisms

In contrast to legged mechanisms, wheel-legged robots are popular when operating in flat environments that require interactions such as pick-and-place. In these cases, robots typically employ two-link folding mechanisms to elevate the robot quickly between target positions. The BHR-W, Ascento, SUSTech-Nezha II, and SR600 are three research-focused examples of this (Lingxuan et al., 2021; Klemm et al., 2019; Yang et al., 2023; Zhang et al., 2019). They typically have motors using bevel gears or pulley mechanisms to drive the wheels and to dynamically balance the robot. The remaining motors are generally actuated at the hip joints to control the angle of the torso relative to the hips and to control the knee flexion with cranks and linkages. While dynamic stability is primarily maintained by active wheel control, the elevation mechanism is typically used to adjust the torso's pitch and vertical position to support manipulation or repositioning tasks. Depending on the joint configuration of the hips, they can also allow the two legs to elevate independently (Klemm et al., 2019). However, two-link elevation mechanisms tend to require high-torque motors because the joints must often support the robot's weight directly, especially during slow or quasi-static motions, and mechanical advantage is limited without added complexity such as gearing, linkages, or gravity compensation (Yun et al., 2019). Alternatives such as WLR-3P and WLR-II provide a higher power-to-weight ratio and impact resistance by using hydraulic actuation (X. Li et al., 2023; X. Li et al., 2019). Although this can significantly improve load capacity, it poses engineering challenges such as compactness, leakages, and cooling (X. Li et al., 2023).

Parallel mechanisms

(a) Linear Stewart platform (Kharboutly et al., 2015)

(b) Folding Stewart platform (Raynaud, 2024)

Figure 9: Examples of parallel elevation mechanisms

In robotic elevation, a parallel mechanism refers to a system where the end-effector (base of robot torso) is connected to multiple independent kinematic chains that operate in parallel. An important nuance to identify is that serial mechanisms can also contain parallel components and vice-versa. The Stewart platform is a classic example of a 6-DoFs parallel mechanism, commonly used in motion simulation and robotic positioning due to its high stiffness and precision. It connects a fixed base to a moving platform via three or more independently actuated variable-length struts arranged in parallel. While widely adopted for applications such as flight and driving simulators, its design presents trade-offs, including a limited workspace, coupled degrees of freedom, complex control schemes, and a relatively large footprint (Kharboutly et al., 2015). Some proposals have been made to increase the elevation range (workspace) of the system by using telescopic linear actuators or through using a servo motor Stewart configuration. In the latter, instead of using linear actuators, each two-link chain is controlled by a servo motor. Generally, the links are connected by an unactuated revolute joint and the end-effector by a universal joint, providing the flexibility needed such that the parallel mechanism can afford to it three or more DoFs (Raynaud, 2024). While this mechanism can provide a greater adjustment range, it also has a large swept volume, which may encumber the robots workspace.

4.2 Industrial systems

In industry, robotic elevation mechanisms are typically more diverse in design due to the breadth of applications - from hospital care to high-precision machinery.

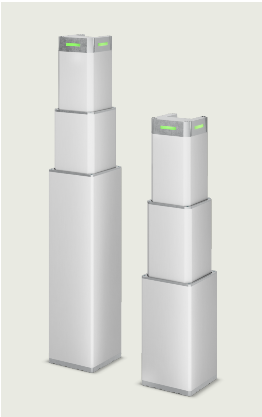

(a) Elevate column (LINAK, 2024)

(b) 1X's Eve (DimensionIA, 2024)

(c) Fetch (Fetch Robotics, 2018)

Figure 10: Examples of industrial elevation mechanisms

A common mechanism is the telescopic spine, which is used in warehouse and house automation robots like Fetch, or the concept robots by Samsung and Toyota (Handy and HSR robots, respectively) (Fetch Robotics, 2018; Samsung Research, 2022; Arima et al., 2025). The telescopic spine offers vertical extension capabilities while maintaining a compact footprint. It is often used in higher precision stationary applications like machining or palletising, such as Linak's Elevate electric lifting column (LINAK, 2024). These systems often excel in stable height adjustment and non-backdriveability but are often slower than folding mechanisms that use servo motors.

Alternatively, articulated mechanisms like 1X's Eve and Dexmate's Vega utilize multi-link folding systems that provide both vertical and horizontal reach adjustability, offering versatility in confined spaces (Humanoid Robots, 2024; Dexmate, 2025). While these designs enable more complex movement patterns, they introduce additional mechanical complexity and potential calibration challenges. The legged locomotion approach of Agility's Digit and Boston Dynamics' Spot represents the most advanced elevation mechanism, allowing navigation over irregular terrain and stairs while maintaining stable elevation—though at significantly higher cost and control complexity compared to wheeled or static solutions (Agility Robotics, 2025; Boston Dynamics, 2025).

5 Architecture selection

To provide an overview of a range of mechanisms that could be used in the elevation mechanism, I introduce 7 different link architectures, chosen based on their feasibility in being integrated into Reachy's current torso and their ability to at least fulfill the two required degrees of freedom for the torso (vertical translation and pitch). These were all identified during the literature and industry review, and they are evaluated using the 13 criteria listed in Table 3.

5.1 Architectures

Figure 11 illustrates the set of potential link architectures that were designed and assembled in OnShape after the literature review, industry benchmark, and open discussions with PR.

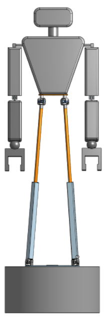
(a) Linear Stewart

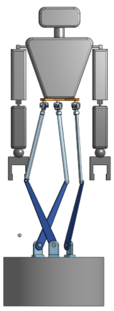
(b) Tri-Stewart

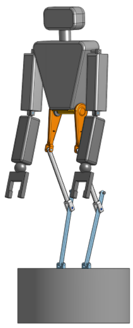
(c) Cassowary


(d) Flea

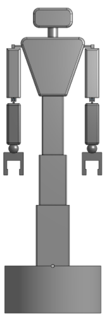
(e) Telescopic

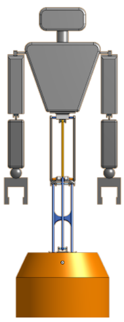
(f) Folding

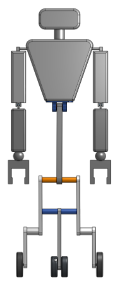
(g) Tri-wheel

Figure 11: Architectural Variants

Linear Stewart

Inspired by an engine simulator, this mechanism (Figure 11a) comprises 4 linear actuators connecting the holonomic base and the torso (S. Li et al., 2022). Depending on the configuration, this mechanism can provide up to 6 DoFs to its end-effector. Additionally, by sharing the end-effector mass, m, between 4 linear actuators the mechanism can support a wide range of loads. For example, the mechanism in the Li et al. paper supports a payload of up to 500 kg. On the other hand, the mechanism's design suggests the robot may struggle to interact with the ground, since linear actuators typically have a minimum height exceeding that of their stroke range. In this respect, possible solutions would be to lower the attachment point of the cylinders beneath the base or use telescopic actuators.

Tri-Stewart

The Tri-Stewart platform (Figure 11b) is inspired by the work of Alexis Raynaud for PR in 2024 (Raynaud, 2024). It consists of three motors spaced equally on the holonomic base at 60 degree angles to each other, forming a triangular pattern. Each motor is attached to the torso via two links, a revolute knee joint, and a universal hip joint. The mechanism can afford three DoFs to the end-effector and provide a sufficient height adjustment range to fulfill the target specification for Δz_{ee} and $z_{ee,min}$, but may be less suitable for integration with the Reachy platform due to the leg obstructions. At a small scale, as in the Raynaud paper, where the radius of the motor trio is similar to the links, there is little obstruction during a complete motion. However, when longer links are used with a narrower base, the links tend to extend far outwards risking collisions with Reachy's arms.

Cassowary

The Cassowary mechanism (Figure 11c) is inspired by Cassie, a bipedal robot developed by Agility Robotics, which is in turn designed to mimic the biomechanics of the Cassowary's legs (Reher et al., 2019). While the original design has multiple motors at the hip joint to afford abduction, rotation, and flexion, my mechanism provides just revolute joints with axes of rotation in the y-direction (to the robots left). This limits its range of motion to two dimensions, affording only pitch and x-z planar translation to the torso. While this simplifies the design, it also means that there is no need for the individual legs to move independently. Furthermore, the Cassie mechanism has a dedicated motor for the knee joint and passive springs between the knee and ankle to improve energy efficiency during the gait cycle. Again, this type of motion is not required for the Reachy robot, meaning the use of springs and the motor placement would need to be reconsidered.

Flea

The Flea mechanism (Figure 11d) is inspired by the 3-RUU mechanism introduced by Yun et al. in 2019, which consists of three identical revolute-universal-universal link chains arranged in a cyclical symmetry (L. Li et al., 2020). My mechanism would mount the system upside-down, with its fixed base securely attached to the top of the holonomic base. From there, three articulated limbs extend upward, each starting with a revolute joint (driven by a motor) followed by two passive universal joints, connecting to a rigid platform that supports the humanoid torso. This setup allows the torso to smoothly rise, lower, and shift in three-dimensional space while maintaining a stable orientation. Similarly to the Tri-Stewart mechanism, this design results in large working volumes, meaning the legs are likely to obstruct Reachy's arms.

Telescopic

The Telescopic mechanism (Figure 11e) is the simplest out of the 7, inspired by industrial applications of robotic manipulators. The Elevate telescopic column by Linak was particularly relevant, as it is used as an elevation mechanism for cobot palletisers, (LINAK, 2024). Consisting of three packed columns that move relative to each other using linear actuators, the design can feasibly reach a $\dot{z}_{ee} = 100\,\mathrm{mm/s}$ with a sufficient payload capacity. However, the simplicity of the design means it requires an extension at the top to afford further DoFs than vertical translation, and even with telescopic columns few models exist on the market with a sufficiently low $z_{ee,min}$.

Folding

The Folding mechanism (Figure 11f) is inspired by the 3-DOF mechanism in Yun et al., which describes a height adjustment mechanism built into a gravity compensation system (Yun et al., 2019). My structure comprises two closed-loop kinematic chains that together make up a planar height adjustment system. The two loops are designed to fold into each other using revolute joints at the base and knee. This makes it able to translate both in the z and x direction. Moreover, using an extra link at the base of the hip, the robot is able to adjust its pitch with a single actuator.

Tri-wheel

Finally, the Tri-wheel (Figure 11g) is different to the other mechanisms in that it strays away from the use of the holonomic base. While this would require significant redesigns for batteries, locomotion, and electronics, PR engineers did express an interest in exploring new locomotion opportunities. Therefore, this design was included to open up for discussions. The mechanism itself is inspired by Aerobot, which is a hybrid leg mechanism that integrates wheels into its links (Otubela and McGinn, 2020). My design includes three actuated wheels that account for a part of the height adjustment and an extra torso link that connects the waist and knee, allowing both for pitch and planar translation.

5.2 Comparative evaluation

Based on the criteria described in Table 3 and scoring logic described in Appendix 10.1, 10.2, and 10.3, I evaluated each mechanism. Figure 12 illustrates the unweighted scores provided to each mechanism for the 13 criteria.

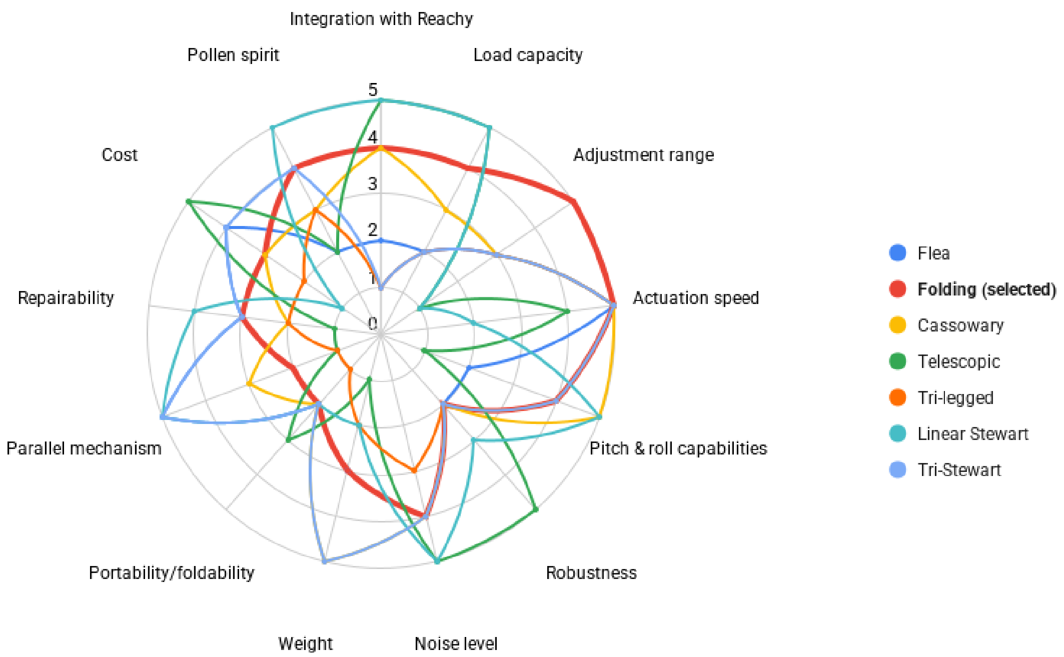

Figure 12: Radar chart of unewighted scores for each architecture

While there were significant variations between the scores in different criteria for each mechanism, several mechanisms were quickly abandoned due to them not feasibly fulfilling the minimum requirements in Table 2. While presenting my findings to the team at Pollen Robotics, it became clear that the preferred architecture was the Folding mechanism, which also scored the highest weighted total of the 7 as shown in Table 4. This suggests that my scoring aligned with the criteria preferred by the PR engineers.

Mechanism	**Total Weighted Score (of 144)**
Linear Stewart	88
Tri-Stewart	82
Cassowary	87
Flea	77
Telescopic	86
Folding	**94**
Tri-wheel	61

Table 4: Total Weighted Scores by Mechanism

6 Theoretical background

This section describes the theory required to understand typical manipulator kinematics concepts used in robotics, which may help understand the analyses conducted in Section 7.

6.1 Kinematic chain typology

Kinematic chain typology refers to the classification of mechanical linkages based on their configuration and mobility (Grossard, 2025). Broadly, mechanisms can be classified as:

- **Open chains**: Kinematic chains that are connected end-to-end in a serial fasion.
- **Closed chains**: Kinematic loops where the end of one chain connects back to a previous link. Parallel mechanisms are often closed chains.

6.2 Denavit-Hartenberg parametrization

In order to model the spatial relationships between serial links in a robotic or mechanical system, the Denavit–Hartenberg (D–H) convention is widely used. The D–H parametrization begins by assigning coordinate frames to each joint of the serial manipulator. For revolute joints, the z-axis (z_{i-1}) of each frame is aligned with the axis of rotation of joint i, which is also the direction of motion. Then, the x-axis (x_i) is defined to be perpendicular to both z_{i-1} and z_i and points along their common normal (i.e., the shortest line connecting them), completing the frame definition according to the right-hand rule. To describe the transformation from frame $i-1$ to frame i, four parameters are assigned at each joint:

- θ_i: Joint angle – the rotation about z_{i-1} between x_{i-1} and x_i.
- d_i: Link offset – the translation along z_{i-1} between the origins of frames $i-1$ and i.
- a_i: Link length – the translation along x_i from z_{i-1} to z_i.
- α_i: Link twist – the rotation about x_i between z_{i-1} and z_i.

6.3 Forward kinematics

Forward kinematics involves computing the pose of an end-effector given a set of joint parameters $\{\theta_1, \theta_2, \ldots, \theta_n\}$. This is achieved by multiplying the sequence of transformation matrices from the base to the end-effector:

$$T_0^n = T_0^1 T_1^2 \ldots T_{n-1}^n$$

The resulting matrix T_0^n encodes the rotation and translation of the end-effector relative to the base frame (Grossard, 2025). This is why D-H is popular for serial mechanisms, as it simplifies the process of deriving individual homogeneous transformation matrices. For example, from frame $i-1$ to frame i the matrix is:

$$T_i^{i-1} = \begin{bmatrix} \cos\theta_i & -\sin\theta_i\cos\alpha_i & \sin\theta_i\sin\alpha_i & a_i\cos\theta_i \\ \sin\theta_i & \cos\theta_i\cos\alpha_i & -\cos\theta_i\sin\alpha_i & a_i\sin\theta_i \\ 0 & \sin\alpha_i & \cos\alpha_i & d_i \\ 0 & 0 & 0 & 1 \end{bmatrix} \quad (4)$$

For planar revolute link mechanisms like the one described in this report, the matrix can be further simplified as all $\alpha_i = 0$.

6.4 Inverse kinematics

Inverse kinematics is the process of determining the joint variables, θ, required to reach a given end-effector pose $\mathbf{x}$. This problem is generally more complex than forward kinematics and may not always have a closed-form solution. For planar two-DoF systems, however, closed-form solutions are often achievable by analytical calculations.

When an analytical solution is difficult or impossible to obtain, the inverse kinematics can be formulated as a numerical optimization problem. It typically starts with a forward kinematics function $f(\boldsymbol{\theta})$ that maps a set of joint parameters $\boldsymbol{\theta} \in \mathbb{R}^n$ to the corresponding end-effector pose $\mathbf{x} \in \mathbb{R}^m$. Using this, the goal is to find an $\boldsymbol{\theta}^*$ such that:

$$\boldsymbol{\theta}^* = \arg\min_{\boldsymbol{\theta}} \|f(\boldsymbol{\theta}) - \mathbf{y}_d\|^2$$

In this example, the squared Euclidean norm of the error is used. Optimization techniques such as gradient descent or sequential quadratic programming (SQP) are commonly employed. These methods can incorporate joint limits, task constraints, and regularization terms, making them suitable for a wide range of robotic systems (Grossard, 2025). The optimization problem is then solved using constrained numerical solvers such as Sequential Least Squares Programming (SLSQP), subject to joint bounds:

$$\theta_i^{\min} \leq \theta_i \leq \theta_i^{\max}, \quad i = 1, 2, 3$$

This method iteratively minimizes the pose error and is particularly useful when analytical solutions are sensitive to numerical instability or constraints.

6.5 Dynamics

The Jacobian matrix, $J(\boldsymbol{\theta})$, describes how joint velocities map to the Cartesian velocity of a point of interest, such as the end-effector:

$$\mathbf{v}_{ee} = J(\boldsymbol{\theta})\, \dot{\boldsymbol{\theta}}$$

where $\mathbf{v}_{ee}$ is the linear and angular velocity of the end-effector, and $\dot{\boldsymbol{\theta}}$ is the vector of joint velocities.

For acceleration, the relationship becomes:

$$\dot{\mathbf{v}}_{ee} = J(\boldsymbol{\theta})\, \ddot{\boldsymbol{\theta}} + \dot{J}(\boldsymbol{\theta})\, \dot{\boldsymbol{\theta}}$$

where $\ddot{\boldsymbol{\theta}}$ is the vector of joint accelerations and $\dot{J}(\boldsymbol{\theta})$ is the time derivative of the Jacobian matrix. Given a desired end-effector velocity or acceleration, the corresponding joint velocities and accelerations can be computed using:

$$\dot{\boldsymbol{\theta}} = J^{-1}(\boldsymbol{\theta})\, \mathbf{v}_{ee}$$

$$\ddot{\boldsymbol{\theta}} = J^{-1}(\boldsymbol{\theta}) \left(\dot{\mathbf{v}}_{ee} - \dot{J}(\boldsymbol{\theta})\, \dot{\boldsymbol{\theta}} \right)$$

6.6 Load analysis

Load analysis evaluates the forces and torques acting on a mechanism due to motion, gravity, and external loads. For static systems, equilibrium is used to solve for the net forces and torques on the links and joints. For dynamic systems, inverse dynamics methods, such as the Newton-Euler approach, are required to compute the joint torques needed to follow a given trajectory (Grossard, 2025). This typically involves a forward pass to determine the velocities and accelerations of each link, followed by a backward pass to propagate forces and torques from the end-effector to the base.

In this analysis, the gravitational and inertial forces acting on each link's center of mass are mapped to joint torques using the corresponding Jacobian matrices.

Gravitational torque

The gravitational torque vector, $\boldsymbol{\tau}^{(g)} \in \mathbb{R}^n$ is computed as:

$$\boldsymbol{\tau}^{(g)} = J_{\text{COM}}^T(\boldsymbol{\theta})\,\mathbf{F}_g$$

where, assuming movement solely in the xz-plane:

- $\mathbf{F}_g \in \mathbb{R}^{2n}$ is the stacked vector of gravitational forces acting at the center of mass of each link (with $[F_{x,i}, F_{z,i}]^T$ for each link i).
- $J_{\text{COM}} \in \mathbb{R}^{2n\times n}$ is the stacked Jacobian matrix that relates joint velocities $\dot{\boldsymbol{\theta}} \in \mathbb{R}^n$ to the Cartesian velocities of all link COMs in the plane.
- n is the number of joints/links (here, $n = 3$ for a planar 3-link manipulator).

For example, for three links in the xz-plane:

$$\mathbf{F}_g = \begin{bmatrix} 0 \\ -m_1 g \\ 0 \\ -m_2 g \\ 0 \\ -m_3 g \end{bmatrix} \in \mathbb{R}^6$$

and

$$J_{\text{COM}} = \begin{bmatrix} J_{\text{COM},1} \\ J_{\text{COM},2} \\ J_{\text{COM},3} \end{bmatrix} \in \mathbb{R}^{6\times 3}$$

where each $J_{\text{COM},i} \in \mathbb{R}^{2\times 3}$ is the Jacobian for the ith link's center of mass. Specifically it looks like:

$$J_{\text{COM},i}(\boldsymbol{\theta}) = \begin{bmatrix} \frac{\partial x_{\text{COM},i}}{\partial \theta_1} & \frac{\partial x_{\text{COM},i}}{\partial \theta_2} & \frac{\partial x_{\text{COM},i}}{\partial \theta_3} \\ \frac{\partial z_{\text{COM},i}}{\partial \theta_1} & \frac{\partial z_{\text{COM},i}}{\partial \theta_2} & \frac{\partial z_{\text{COM},i}}{\partial \theta_3} \end{bmatrix}$$

where $x_{\text{COM},i}$ and $z_{\text{COM},i}$ are the x and z positions of the ith link's center of mass as functions of the joint angles.

Inertial torque

The second torque component that I analyze is the inertial torque of the links throughout a motion profile. The inertial torque at joint i includes both the torque needed to accelerate the link's own rotational inertia about the joint and the torque needed to accelerate the mass of the link (and any payload) through space. This can be expressed as:

$$\tau_i^{(in)} = I_i\,\ddot{\theta}_i + \mathbf{r}_{\text{COM},i} \times m_i\,\ddot{\mathbf{r}}_{\text{COM},i}$$

where:

- I_i is the rotational inertia of link i about its joint axis,
- $\ddot{\theta}_i$ is the angular acceleration of joint i,
- m_i is the mass of link i,
- $\mathbf{r}_{\text{COM},i}$ is the position vector from joint i to the center of mass of link i,
- $\ddot{\mathbf{r}}_{\text{COM},i}$ is the Cartesian acceleration of the COM.

Thus, the total inertial torque at all joints can be computed by summing the contributions of all links (including any distal point masses), using the Jacobian-transpose method to map inertial forces at the COMs back to the joint axes:

$$\boldsymbol{\tau}^{(in)} = \sum_{i=1}^{n} \left[I_i\,\ddot{\theta}_i + J_{\text{COM},i}^T(\boldsymbol{\theta})\,m_i\,\ddot{\mathbf{r}}_{\text{COM},i} \right]$$

Note that in this case I do not include the effects of motor inertia because, at such an early stage of analysis, their contribution is typically small compared to the inertial effects of the links themselves and can be neglected for simplicity. These effects can be added later if higher fidelity is required.

Total torque

The total torque τ_i at each joint is composed of two components:

$$\tau_i(t) = \tau_i^{(g)}(t) + \tau_i^{(in)}(t)$$

7 Kinematic and dynamic analysis

As the Folding mechanism was selected for further analysis, this section provides a more mathematical study of its link structure. As Figure 13 suggests, the mechanism has two planar closed-loop kinematic chains. The purpose of this mechanism is to automatically adjust the height of Reachy's torso so that it may interact with elevated and ground-level objects without manual interference. In Section 2 I defined the key targets mathematically, as summarized in Table 2. These values help determine the expected kinematic and dynamic properties of the mechanism. To start, I simplify the closed loop kinematic structures by representing them as simple parametrized links in a 2D plane, illustrated in Figure 14.

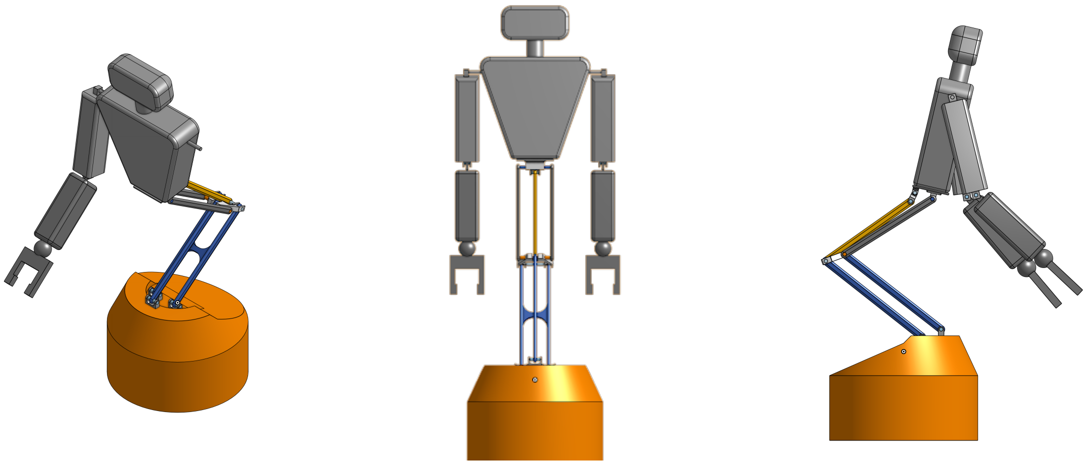

Figure 13: Folding mechanism: isometric view (without the left arm for visibility), front view, and side view.

7.1 Kinematic analysis

The first step is to define the Folding mechanism as a simple serial link chain, as illustrated in Figure 14.

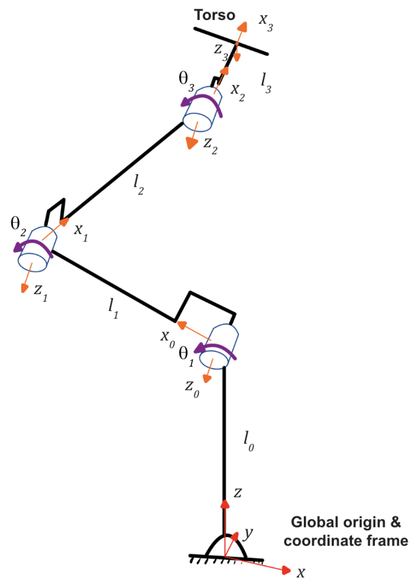

Joint i	$\theta_i\,(z:x)$	$d_i\,(z)$	$r_i\,(x)$	$\alpha_i\,(x:z)$
J1	θ_1	0	l_1	0
J2	θ_2	0	l_2	0
J3	θ_3	0	l_3	0

Legend:

- $(z:x)$: angle in x_{i-1}, x_i about z_{i-1}
- (z): offset along z_{i-1}
- (x): distance along x_i
- $(x:z)$: angle in z_{i-1}, z_i about x_i

Figure 14: (Left) Frame assignment for the simple serial chain. Each frame is at the center of the joint. (Right) Corresponding Denavit-Hartenberg parameters.

The kinematic model in Figure 14 presents a parametrized version of the simple structure, where $l_0 = h_{\text{base}} + h_{\text{ext}}$ and $l_3 = l_{\text{ext}}$. In this structure l_0 is fixed in space, and the three links l_1, l_2, and l_3 can rotate around their respective joints, which is why they are the only ones described in the D-H parameters. The angles θ_1, θ_2, and θ_3 describe the joint angles based on D-H conventions.

Forward kinematics

In order to define the forward kinematics of the simple structure from the global (base) coordinate frame at ground level, I start with a translation and rotation to the first joint. The translation and rotation are defined by the following transformation matrices:

$$T_{base} = \begin{bmatrix} 1 & 0 & 0 & 0 \\ 0 & 1 & 0 & 0 \\ 0 & 0 & 1 & l_0 \\ 0 & 0 & 0 & 1 \end{bmatrix}, \quad T_{rotate} = \begin{bmatrix} 1 & 0 & 0 & 0 \\ 0 & 0 & -1 & 0 \\ 0 & 1 & 0 & 0 \\ 0 & 0 & 0 & 1 \end{bmatrix}$$

Using the D-H parameters to get the frame-to-frame transformation matrices, the complete transformation from base to end-effector is:

$$T_{\text{base}}^{\text{EE}} = \underbrace{T_{\text{base}}}_{\text{z-translation by } l_0} \cdot \underbrace{T_{\text{rotate}}}_{\text{align to xz-plane}} \cdot T_0^1 \cdot T_1^2 \cdot T_2^3 \tag{5}$$

Note that it is also possible to do this transformation manually:

$$\begin{aligned} x_{ee}(\boldsymbol{\theta}) &= l_1 \cos\theta_1 + l_2 \cos(\theta_1 + \theta_2) + l_3 \cos(\theta_1 + \theta_2 + \theta_3) \\ z_{ee}(\boldsymbol{\theta}) &= l_0 + l_1 \sin\theta_1 + l_2 \sin(\theta_1 + \theta_2) + l_3 \sin(\theta_1 + \theta_2 + \theta_3) \\ \varphi_{ee}(\boldsymbol{\theta}) &= \theta_1 + \theta_2 + \theta_3 \end{aligned} \tag{6}$$

Jacobian

To calculate the Jacobian, $J(\boldsymbol{\theta})$, of the mechanism I take the partial derivatives of the forward kinematics in Equation 6.

$$J(\boldsymbol{\theta}) = \begin{bmatrix} \frac{\partial x_{ee}}{\partial\theta_1} & \frac{\partial x_{ee}}{\partial\theta_2} & \frac{\partial x_{ee}}{\partial\theta_3} \\ \frac{\partial z_{ee}}{\partial\theta_1} & \frac{\partial z_{ee}}{\partial\theta_2} & \frac{\partial z_{ee}}{\partial\theta_3} \\ \frac{\partial \varphi_{ee}}{\partial\theta_1} & \frac{\partial \varphi_{ee}}{\partial\theta_2} & \frac{\partial \varphi_{ee}}{\partial\theta_3} \end{bmatrix} = \begin{bmatrix} -l_1S_1 - l_2S_2 - l_3S_3 & -l_2S_2 - l_3S_3 & -l_3S_3 \\ l_1C_1 + l_2C_2 + l_3C_3 & l_2C_2 + l_3C_3 & l_3C_3 \\ 1 & 1 & 1 \end{bmatrix}$$

where I make the following abbreviations:

$$S_i = \sin\Theta_i, \quad C_i = \cos\Theta_i$$

$$\Theta_1 = \theta_1, \quad \Theta_2 = \theta_1 + \theta_2, \quad \Theta_3 = \theta_1 + \theta_2 + \theta_3$$

Singularities

Calculating the values of $\boldsymbol{\theta}$ for which $\det(J(\boldsymbol{\theta})) = 0$ reveals several singularities in this simple mechanism. Two of these occur when $\theta_2 = 0°$ and $\theta_2 = 180°$ as these represent the fully extended and fully folded orientations, respectively. Thus, these two positions should be avoided.

Motion profile

For this analysis, I set the link lengths as $l_0 = h_{\text{base}} + 0.05 = 0.2901\,\text{m}$, $l_1 = 0.4\,\text{m}$, $l_2 = 0.4\,\text{m}$, and $l_3 = 0.05\,\text{m}$. This selection was made to fulfill the stroke range requirement, yet they are still parameters that can be modified. To visualize the attainable workspace of this mechanism under no θ constraints, I plotted 10000 random configurations in Figure 15.

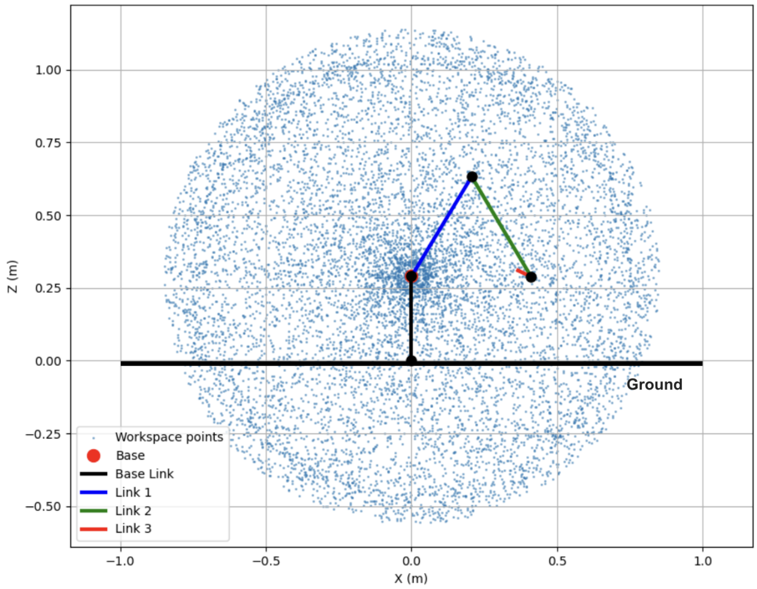

Figure 15: Unrestricted 2D workspace

This figure clearly illustrates the need to constrain the path to ensure that the robot follows the motion profile described in Section 2.5, and to avoid physical constraints like the ground and interfering components. To solve this, I started by constraining θ_1 to $(90°, 270°]$ to account for the symmetry over the z-axis. Then I applied the end-effector bang-bang motion profile from Section 2.5 using inverse kinematics to determine the joint configuration at each point. Figure 16 illustrates 7 steps of the motion profile at three possible pitches.

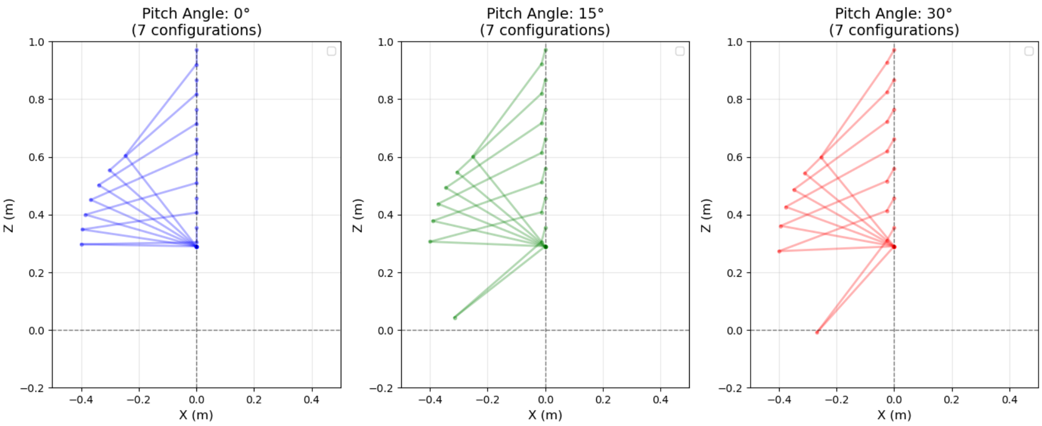

Figure 16: Restricted trajectory for pitches a. 0°, b. 15°, and c. 30°

At a pitch angle of 15° and 30°, the lowest point in the trajectory sees the links folding below the height of l_0, which would have implications on the design of links 1 and 2, and the holonomic base. Modifying the link lengths can minimize this issue.

7.2 Dynamic analysis

To assess the dynamic performance of the folding mechanism with the motion profile in Figure 16a during its vertical end-effector motion, the motion was generated between $z_0 = 0.3541\,\text{m}$ and $z_f = 0.9701\,\text{m}$ over a time period of $T_f = 10\,\text{s}$, with a maximum velocity $v_{\max} = 0.1\,\text{m/s}$ and maximum acceleration $a_{\max} = 0.025\,\text{m/s}^2$. The selection of this trajectory was made as I assumed a design choice wherein Reachy's torso is vertical during elevation.

Using inverse kinematics, the joint angles corresponding to the desired vertical trajectory were computed in Section 7.1. From this, joint velocities and accelerations were derived using numerical differentiation and the Jacobian-based formulation:

$$\dot{\boldsymbol{\theta}} = J^{-1}(\boldsymbol{\theta})\,\dot{\mathrm{x}}, \quad \ddot{\boldsymbol{\theta}} = J^{-1}(\boldsymbol{\theta})\left(\ddot{\mathrm{x}} - \dot{J}(\boldsymbol{\theta})\,\dot{\boldsymbol{\theta}}\right)$$

where $\dot{J}$ was approximated using centered finite differences over the trajectory. This resulted in the dynamic profile over the 10 second motion illustrated in Figure 17.

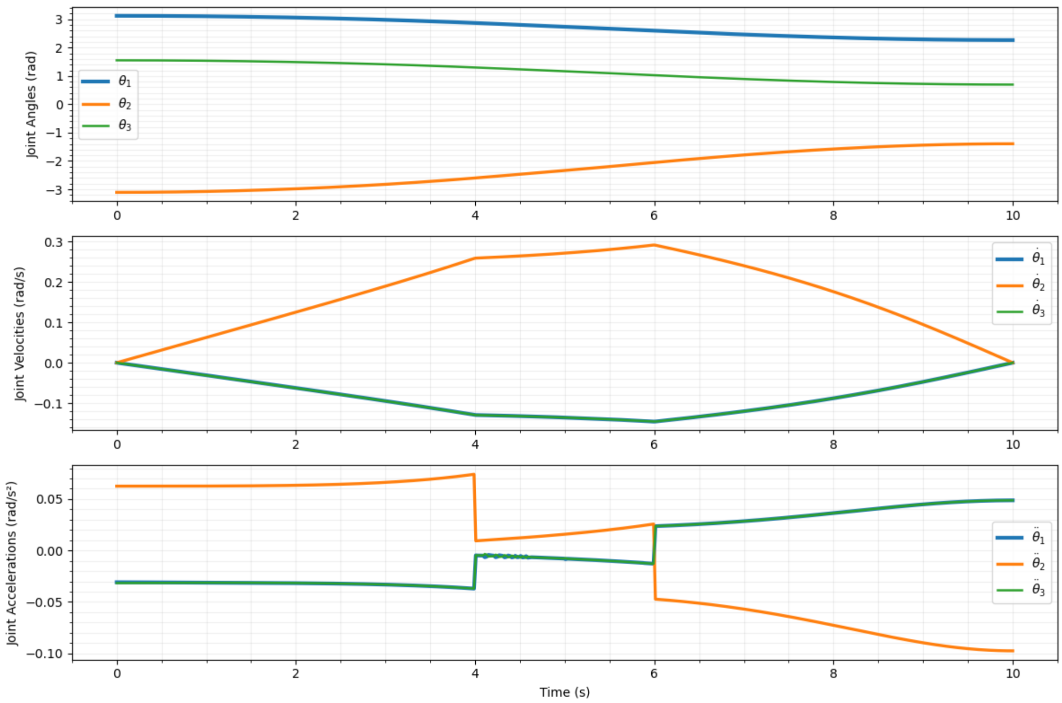

Figure 17: Joint space dynamics over the vertical trajectory. Top: joint angles $\theta_i(t)$, middle: velocities $\dot{\theta}_i(t)$, bottom: accelerations $\ddot{\theta}_i(t)$.

The sharp jumps observed in the joint accelerations are a direct result of the bang-bang motion profile used for the end-effector trajectory. This profile causes abrupt changes (jerk) in the end-effector acceleration at the switching points. These discontinuities in $\ddot{\mathbf{x}}$ are mapped into the joint space by the Jacobian, resulting in step changes in $\ddot{\boldsymbol{\theta}}$. In theory, these jumps represent instantaneous changes and would be infinite (impulses), but in practice they appear as large finite steps due to the discrete time resolution and numerical differentiation of the Jacobian. For later analyses, S-curve motion profiles exhibit less abrupt behavior.

As for the joint angles, they are far from singular points across the motion profile and appear to remain within expected joint limits.

Moreover, I extracted the maximum values from these dynamic trajectories to get approximates for $|\dot{\theta}_{i,max}|$ and $|\ddot{\theta}_{i,max}|$.

$$|\dot{\boldsymbol{\theta}}_{\max}| = \begin{bmatrix} 0.146 \\ 0.292 \\ 0.146 \end{bmatrix} \text{ rad/s}, \quad |\ddot{\boldsymbol{\theta}}_{\max}| = \begin{bmatrix} 0.049 \\ 0.097 \\ 0.049 \end{bmatrix} \text{ rad/s}^2$$

7.3 Torque analysis

In order to determine the torque on each joint, I model the forces acting on the folding mechanism during motion, including gravity and inertial effects from the prescribed acceleration profile. In this initial analysis, the effect of motor rotor inertia, reflected through the gear ratio, is neglected at this stage to provide a first-order estimate of joint torques. For this, I treat each link as a uniform rigid body with known mass and moment of inertia. Let m_i and I_i be the mass and rotational inertia (about the joint axis) of link i, and let $g = 9.81\,\mathrm{m/s}^2$ denote gravitational acceleration. The center of mass (COM) of each link is located at its midpoint, i.e., at a distance $l_i/2$ from the preceding joint along the link direction. Using the joint accelerations derived earlier and assuming link parameters $m_1 = m_2 = 1\,\mathrm{kg}$, $m_3 = 0.3\,\mathrm{kg}$, and uniform density, I numerically evaluated the torques at each joint over time. Moreover, the mass of the end-effector $m = 40.77\,\mathrm{kg}$ is simply assumed to be a point mass at $l_{\mathrm{torso}/2}$ above the end-effector. My calculations followed the approach of separately computing inertial and gravitational torque, as described in Section 6.6. Figure 18 shows the torque trajectories for the motion profile in Figure 16a.

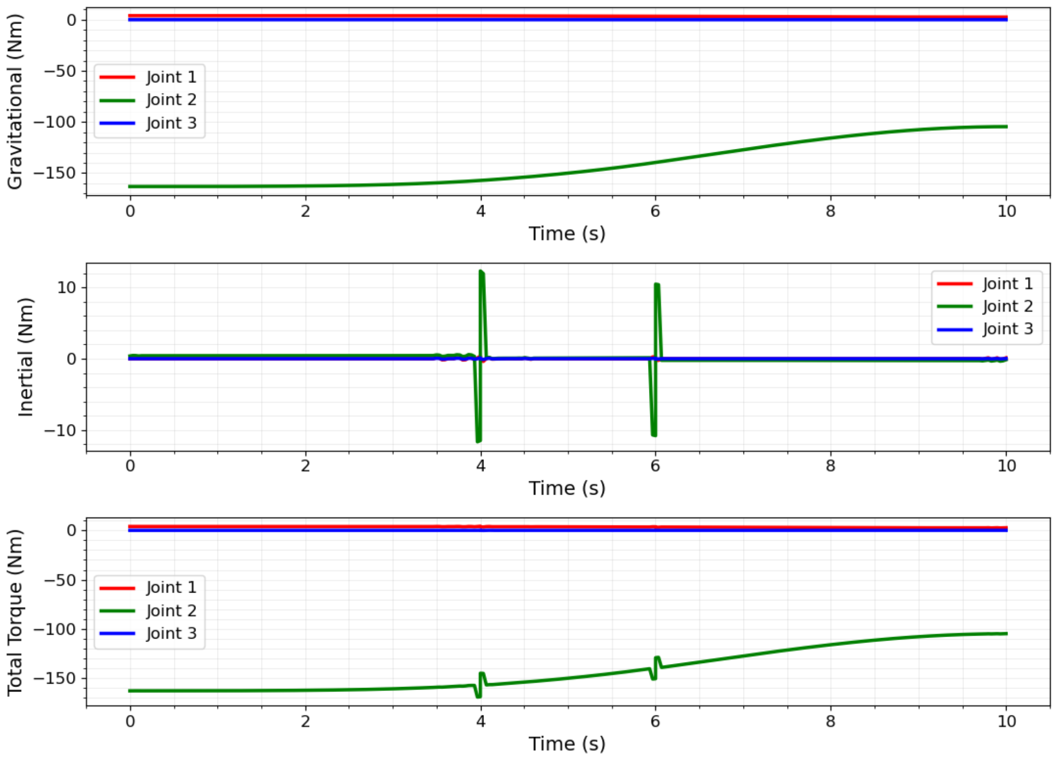

Figure 18: Joint torques over time for the vertical trajectory.

The maximum torque for each joint along the motion profile is:

$$|\boldsymbol{\tau}_{\max}| = \begin{bmatrix} 3.45 \\ 143.25 \\ 0.02 \end{bmatrix} \text{ Nm}$$

These results align with what could be expected intuitively. As the motion of the end-effector is vertically above joint 1 and 3, it does not exert much gravitational torque on it, and most of the torque for these joints come from the moments of intertia. However, as joint 2 extends behind $x = 0$, most of its torque is caused by the torso's mass.

While the assumption was that elevation would occur at a pitch of $\phi = 0°$, I also calculated the maximum torques in the worst-case scenario; elevation at $\phi = 30°$. This gave the following results:

$$|\boldsymbol{\tau}_{\max,worst}| = \begin{bmatrix} 22.45 \\ 198.91 \\ 37.14 \end{bmatrix} \text{ Nm}$$

8 Discussion

In this section I discuss the results of the detailed analysis and elevate potential practical solutions to some of the issues it raises. Ultimately, this should help PR make modifications that align with my proposed targets and design vision.

8.1 Closed chain

An approach that could be used to spread the torque load on multiple joints and even to simplify the model needed to maintain the torso parallel to the ground is with a parallel link structure, as illustrated in Figure 19.

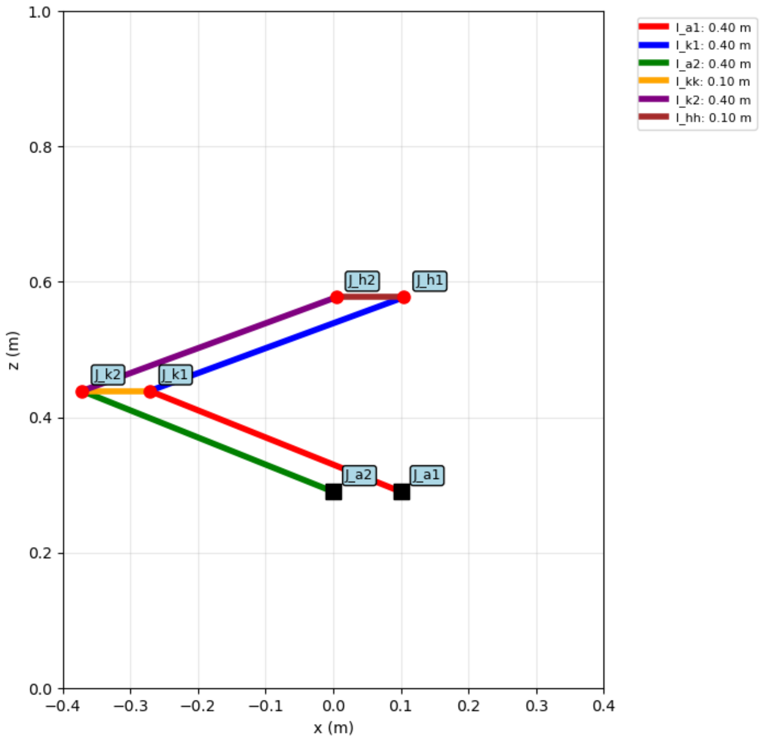

Figure 19: Parallelogram closed chain structure.

The advantage of this structure is that it enforces the top plate on which the torso sits to be parallel to the ground. Any subsequent pitch mechanism attached to this plate would, thus, not need to compensate for the pitches causes by elevation changes in the simple serial mechanism. Moreover, by extending this structure into three dimensions, as exemplified in Figure 13, the torque can be shared amongst multiple actuators in the y-axis.

8.2 Gravity compensation

A major disadvantage of both mechanisms illustrated so far is how much torque the torso's weight exerts on the knee joint(s). At both the knee and ankle joints, efforts should be made to design gravity compensation mechanisms that ensure equilibrium when the structure is static. Yun et. al. describe their use of a 1 DoF spring-based gravity compensation mechanism to achieve this (Yun et al., 2019). The concept is simply illustrated in Figure 20.

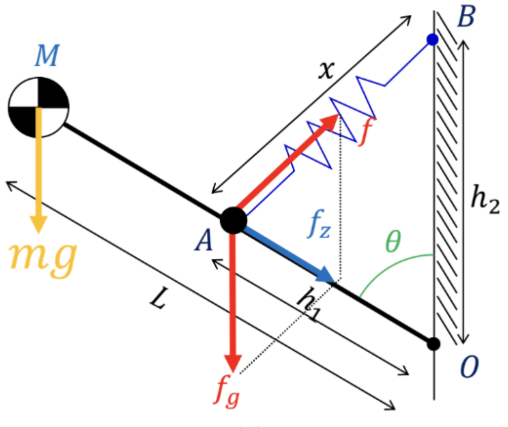

Figure 20: Gravity compensation sketch (Yun et al., 2019).

The gravitational torque on a link is $\tau = mgl \sin\theta$ where m, l, and θ are the mass, length, and joint angle, respectively. After a few substitutions, the following formula can be used to determine the spring stiffness:

$$k = \frac{f}{x} = \frac{mgL}{h_1 h_2}$$

This design assumes a spring with an untensioned length of 0. As such a spring does not exist, it can be realized using a compression spring, which is described in detail in Yun et al., 2019. As such, there are design decisions that can be made to counteract the mass of the robot. I provide one possible conceptual sketch of gravity compensation in Figure 21.

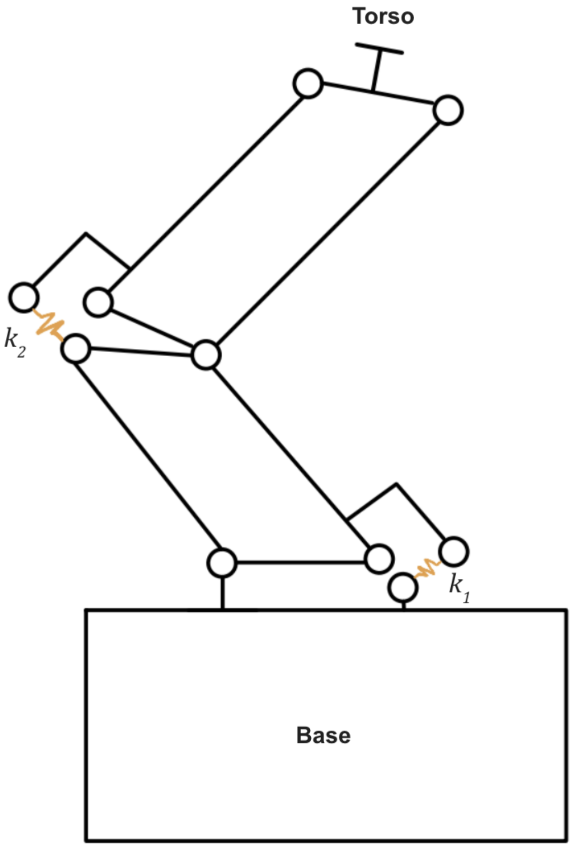

Figure 21: Sample sketch of gravity compensation for the parallelogram architecture.

In this figure, k_1 and k_2 represent the spring constants for two potential gravity compensation springs, which are expected to fall within the range of 5 kN/m to 10 kN/m. These are reasonable values for many spring types and can be calculated more precisely once the detailed geometry of the mechanism is finalized.

8.3 Actuation

The choice of actuator is central to achieving the necessary force, speed, and control precision for the proposed mechanism. In this mechanism the choice lies between linear actuators and rotary motors.

Rotary motors, particularly when coupled with harmonic drives or gearboxes with high reduction, are more commonly used in robotic joints and offer mature control frameworks. Their rotational output can be directly used in serial mechanisms. This means that their placement near the revolute joints in the aforementioned designs is feasible. However, it should be noted that it might not be possible to use the standard Maxon motors that Pollen Robotics typically uses (Pollen Robotics, 2025c). While smaller motors with a high torque ratio may be feasible with a gravity compensation system in place, I suggest this as a future work in relation to this report.

Alternatively to the rotary motors, linear actuators offer direct control over linear displacement, which can be beneficial in mechanisms where linear motion is either the desired output or more easily translated into the required angular motion via linkages. With a parallelogram-style setup, I believe linear actuators could feasibly be attached between the robotic base and along the link near J_{a2} or J_{a1}, and similarly between the link connecting J_{k2} and J_{k1}, and along the link near J_{k2}. These joints are illustrated in Figure 19. The challenge in this design will be ensuring a sufficiently low extension can be reached for the end-effector to drop to its lowest positions.

It is also possible to explore a hybrid approach, in which linear actuators act as the primary lifting mechanism, and rotary motors for fine pitch adjustments, offering the best balance between structural simplicity and performance.

9 Conclusion

Designing an elevation link mechanism for platforms like Reachy requires a detailed understanding of the problem to be solved and an analysis of the potential architectures available to accomplish the task. In this report, I clearly defined the problem space and identified the key targets to fulfill by the mechanisms such as the stroke range, Δz_{ee}, and the load capacity, m. Due to resource constraints, it is difficult to assess all possible architectures in detail, and consequently using heuristics, experience, and basic calculations can suffice in narrowing the search scope. For Reachy, it became evident that the Folding mechanism has the most potential out of the 7 options. Finally, I could investigate the motion profile of the basic folding architecture to determine some preliminary values for joint velocity, accelerations, and torques. From this, I discuss some more practical approaches to solving the issues of torque requirements and pitch management. In general, I suggest further investigating the details of the Folding mechanism, paying particular attention to gravity compensation designs and actuation methods.

References

Agility Robotics. (2025). Digit [Accessed: 2025-05-03]. https://www.agilityrobotics.com/

Alpha Motor Corporation. (2020). EV vs. ICE: Fewer Moving Parts, Less Maintenance [Accessed: 2025-05-13]. https://www.alphamotorinc.com/about/ev-vs-ice-fewer-moving-parts-less-maintenance

Arima, J., Takaba, Y., & Wakayama, Y. (2025). Frontier research [Accessed: 2025-05-03]. https://global.toyota/en/mobility/frontier-research/42394425.html

Auxiliary spring applications. (2017). 4x4 Styling. https://www.4x4styling.com/Auxiliary-Springs-Airsprings

Bjelonic, M., Klemm, V., Lee, J., & Hutter, M. (2023). A survey of wheeled-legged robots. In J. M. Cascalho, M. O. Tokhi, M. F. Silva, A. Mendes, K. Goher, & M. Funk (Eds.), *Robotics in natural settings* (pp. 83–94). Springer International Publishing.

Boston Dynamics. (2025). Spot: The agile mobile robot [Accessed: 2025-05-03]. https://bostondynamics.com/products/spot/

Chen, B., Xu, Q., Zhu, B., Yang, Y., & Li, Y. (2022). Buckling and postbuckling behaviors of symmetric/asymmetric double-beam systems. *International Journal of Mechanical Sciences*, *235*, 107712. https://doi.org/https://doi.org/10.1016/j.ijmecsci.2022.107712

Dexmate. (2025). Vega: General-purpose mobile robot [Accessed: 2025-05-03]. https://www.dexmate.ai/vega

Diamandis, P. (2024). *Metatrend robotics* (tech. rep.) (Accessed: 2025-04-01). Windesheim University of Applied Sciences. https://www.windesheim.tech/wp-content/uploads/2024/11/MetaTrend_Robotics-1.pdf

DimensionIA. (2024, January). *1x technologies: Liderando la revolución de la robótica con openai* [Accessed: 2025-05-31]. https://www.dimensionia.com/1x-technologies/

Eaker, M., & Mitra, D. (2020). *How to reduce audible noise in stepper motors* (tech. rep. No. SLVAES8) (Accessed: 2025-05-10). Texas Instruments. https://www.ti.com/lit/an/slvaes8/slvaes8.pdf

Eitel, L., Huebner, M., & Bischel, K. (2020). Linear motion systems only as strong as weakest link [Accessed: 2025-05-10]. https://www.linearmotiontips.com/linear-motion-systems-only-as-strong-as-weakest-link/

Elsevier. (2025). Scopus [Accessed: 2025-05-08].

Fetch Robotics. (2018). Fetch mobile manipulator [Accessed: 2025-05-03]. https://fetchrobotics.borealtech.com/robotics-platforms/fetch-mobile-manipulator/?lang=en

Fu, Z., Zhao, Q., Wu, Q., Wetzstein, G., & Finn, C. (2024). Humanplus: Humanoid shadowing and imitation from humans. *Conference on Robot Learning (CoRL)*.

Google. (2025). Google Scholar [Accessed: 2025-05-08].

Grossard, M. (2025). Interactive robotic systems: Basics of modeling and control [Lecture notes, CentraleSupélec, Interactive Robotics Unit, CEA LIST - Nano-Innov].

Hubicki, C., Grimes, J., Jones, M., Renjewski, D., Spröwitz, A., Abate, A., & Hurst, J. (2016). Atrias: Design and validation of a tether-free 3d-capable spring-mass bipedal robot. *The International Journal of Robotics Research*, *35*(12), 1497–1521. https://doi.org/10.1177/0278364916648388

Humanoid Robots. (2024). Eve [Accessed: 2025-05-03]. https://humanoids.wiki/w/Eve

Hydroma electric motors catalog. (2023). https://www.hydroma.eu/electric-motors/

Hyon, S.-H., Kamijo, S., & Mita, T. (2002). Kenken: A biologically inspired one-legged running robot. *Journal of the Robotics Society of Japan*, *20*(4), 453–462. https://doi.org/10.7210/jrsj.20.453

IEEE. (2025). IEEE Xplore Digital Library [Accessed: 2025-05-08].

Kharboutly, H., Ma, J., Benali, A., Thoumie, P., Pasqui, V., & Bouzit, M. (2015). Design of multiple axis robotic platform for postural stability analysis. *IEEE Transactions on Neural Systems and Rehabilitation Engineering*, *23*(1), 93–103. https://doi.org/10.1109/TNSRE.2014.2329533

Kimbell, G. (2019). How to choose a quiet actuator with a decibel chart [Accessed: 2025-05-10]. https://www.progressiveautomations.com/blogs/how-to/choose-a-quiet-actuator

Klemetson, R. (2020). What's Best: Integrated Linear Actuators or Traditional? [Accessed: 2025-05-13]. https://www.tolomatic.com/blog/whats-best-integrated-linear-actuators-or-traditional/

Klemm, V., Morra, A., Salzmann, C., Tschopp, F., Bodie, K., Gulich, L., Küng, N., Mannhart, D., Pfister, C., Vierneisel, M., Weber, F., Deuber, R., & Siegwart, R. (2019). Ascento: A two-wheeled jumping robot. *2019 International Conference on Robotics and Automation (ICRA)*, 7515–7521. https://doi.org/10.1109/ICRA.2019.8793792

Li, L., Fang, Y., Guo, S., Qu, H., & Wang, L. (2020). Type synthesis of a class of novel 3-dof single-loop parallel leg mechanisms for walking robots. *Mechanism and Machine Theory*, *145*, 103695. https://doi.org/https://doi.org/10.1016/j.mechmachtheory.2019.103695

Li, S., Wang, S., Song, J., Li, H., & Xu, H. (2022). Configuration design and experimental research of parallel mechanism without parasitic motion for engine motion simulation. *IEEE Access*, *10*, 111864–111878. https://doi.org/10.1109/ACCESS.2022.3208561

Li, X., Yu, H., Feng, H., Zhang, S., & Fu, Y. (2023). Design and control for wlr-3p: A hydraulic wheel-legged robot. *Cyborg and Bionic Systems*, *4*, 0025. https://doi.org/10.34133/cbsystems.0025

Li, X., Zhou, H., Zhang, S., Feng, H., & Fu, Y. (2019). Wlr-ii, a hose-less hydraulic wheel-legged robot. *2019 IEEE/RSJ International Conference on Intelligent Robots and Systems (IROS)*, 4339–4346. https://doi.org/10.1109/IROS40897.2019.8967935

LINAK. (2024). Lifting column lc3 ic – data sheet [Accessed: 2025-05-03]. https://cdn.linak.com/-/media/files/data-sheet-source/en/lifting-column-lc3ic-data-sheet-eng.pdf

Lingxuan, Z., Yu, Z., Chen, X., Huang, G., Wang, W., Lianqiang, H., Qiu, X., Zhang, X., & Huang, Q. (2021). System design and balance control of a novel electrically-driven wheel-legged humanoid robot, 742–747. https://doi.org/10.1109/ICUS52573.2021.9641385

Otubela, M. V., & McGinn, C. (2020). Controlling fast height variation of an actively articulated wheeled humanoid robot using center of mass trajectory. *2020 IEEE International Conference on Robotics and Automation (ICRA)*, 1518–1524. https://doi.org/10.1109/ICRA40945.2020.9196569

Pollen Robotics. (2025a). Pollen robotics - developing the future of robotics [Accessed: 2025-04-01]. https://www.pollen-robotics.com/

Pollen Robotics. (2025b). Reachy 2 specifications: Key features, architecture & dimensions [Accessed: 2025-05-25].

Pollen Robotics. (2025c). Screenshot of reachy 2 assembly in onshape [Image captured by the author. CAD model provided by Pollen Robotics via private access on OnShape].

PTC Inc. (2025). Onshape Product Development Platform [Accessed: 2025-05-08].

Raynaud, A. (2024, September). *Développement de modules mécatroniques pour l'extension des fonctions du robot reachy chez pollen robotics* (Rapport de Stage). SIGMA Clermont. Clermont-Ferrand, France.

Reher, J., Ma, W.-L., & Ames, A. D. (2019). Dynamic walking with compliance on a cassie bipedal robot. https://arxiv.org/abs/1904.11104

Samsung Research. (2022). [CES 2022] Samsung Research's New Tech Trio Samsung Bot Handy – Housework robot [Accessed: 2025-05-03]. https://research.samsung.com/news/-CES-2022-Samsung-Research-New-Tech-Trio-Samsung-Bot-Handy-Housework-robot

Smac corporation price guide. (2023). https://www.smac-mca.com/products/price-guide

Taylor, K. (2025, January). Direct-drive vs. belt-drive air compressors: What's better? [Accessed: 2025-05-10]. https://fluidairedynamics.com/blogs/articles/direct-drive-or-belt-driven-air-compressor-what-s-better

Transmission, G. (2024, December 19). *Servo motor cost analysis*. https://www.gian-transmission.com/servo-motor-cost-understanding-the-factors-pricing-models-and-key-considerations/

Wang, B., Zhang, K., Ma, X., & Jia, L. (2024). A compliant leg design combining pantograph structure with leaf springs. *Robotica*, *42*(2), 332–346. https://doi.org/10.1017/S0263574723001443

Yang, Z., Bian, Z., & Zhang, W. (2023). Design and control of multi-mode wheeled-bipedal robot with parallel mechanism. *2023 International Conference on Communications, Computing and Artificial Intelligence (CCCAI)*, 69–74. https://doi.org/10.1109/CCCAI59026.2023.00021

Yun, S.-H., Seo, J., Yoon, J., Song, H., Kim, Y.-S., & Kim, Y.-J. (2019). 3-dof gravity compensation mechanism for robot waists with the variations of center of mass. *2019 IEEE/RSJ International Conference on Intelligent Robots and Systems (IROS)*, 3565–3570. https://doi.org/10.1109/IROS40897.2019.8968046

Zhang, C., Liu, T., Song, S., & Meng, M. Q.-H. (2019). System design and balance control of a bipedal leg-wheeled robot. *2019 IEEE International Conference on Robotics and Biomimetics (ROBIO)*, 1869–1874. https://doi.org/10.1109/ROBIO49542.2019.8961814

10 Appendix

10.1 Criteria definitions

Integration with Reachy 2: How seamlessly the mechanism integrates with the existing hardware platform. This includes the extent to which changes must be made to Reachy's torso, the impact on the design of the holonomic base, and the level of interference the mechanism may incur with Reachy's arms across the elevation envelope.

Static load capacity: The amount of weight that the mechanism can support under worst-case conditions. It should be able to maintain at least 400 N (estimate of Reachy's torso with grasped object) under static loads over extended periods of time without significantly compromising energy use.

Adjustment range: The maximum and minimum achievable height of Reachy's torso by the mechanism. The PR team expects a range of at least 600 mm. In order to interact with ground objects, I calculated an approximate minimal torso height of 233 mm (given no pitch) to comfortably interact with ground-level objects at a 45° angle between the wrist and ground.

Actuation speed: The speed at which the mechanism can elevate or lower the torso. PR engineers stated a minimum time from minimum to maximum height of about 10 seconds, corresponding to approximately 60 mm/s. However, speeds upward of 100 mm/s are preferred.

Pitch & roll abilities: Whether the mechanism already affords pitch and roll at the torso or to what extent the mechanism must be modified to do so. Emphasis is placed on the more important freedom: pitch. Furthermore, this ability should also remain for all levels of elevation.

Robustness: The extent to which the mechanism is likely to break down under normal operating conditions. In an early stage, this is qualified using the best-practice heuristics defined in Appendix 10.3.

Sound level: The expected noise level of the mechanism during normal operation. The PR engineers prefer a quiet system that will not interfere with any onboard microphones. This criterion is qualified using common-sense engineering heuristics as defined in Appendix 10.3.

Weight: The weight of the mechanism itself. It is measured by setting expected materials for joints and links and using fixed estimates for other components like linear actuators, motors, and springs.

Portability: The extent to which the mechanism can easily be transported. This includes considerations like disassembly and foldability. I disregard weight in this criterion to avoid overlap. A common-sense approach is used at this stage by applying the heuristics in Appendix 10.3.

Parallel mechanism: The degree to which the mechanism is parallel. As PR prefers parallel link mechanisms in their engineering ethos, fully parallel or partially parallel mechanisms are preferred over purely serial mechanisms.

Repairability: How feasible it is to repair or replace broken components without specialized tools. Due to the target customer for PR being research labs, it is important that individuals can repair the robot with basic tools and 3D printed parts. I qualify this using typical engineering customs outlined in Appendix 10.3.

Cost: The cost to produce the mechanism. This excludes research and development costs. For the comparative analysis, I use a simple estimate on actuator costs based on off-the-shelf component prices and evaluate material requirements and manufacturing approaches.

Pollen spirit: The degree to which the esthetics of the mechanism agrees with PR's design ethos. The design should be simple, elegant, and user-friendly.

10.2 Criteria calculations

Five of the 13 criteria can already in the comparative analysis of the unactuated mechanism skeletons be supported by approximate calculations. These intend to guide the comparative evaluation of the mechanisms.

Static load capacity estimate

To estimate load capacities between architectures, I compare the strengths of revolute and prismatic joints. Due to the challenges of hydraulic and pneumatic cylinders in humanoid robot applications, I assume all actuators use electric motors. I leave the dynamic analysis of load (including intertial effects) to the detailed analysis of the Folding mechanism.

Revolute joints: As illustrated in Figure 22, a revolute joint requires a torque τ_r to support a static moment of $M = Flcos\phi$. Under the worst-case scenario, in which

I have:

$$l = 1\,\text{m}$$
$$\phi = 0°$$
$$F = 500\,\text{N}$$

I get $\tau_r = 500\,\text{Nm}$.

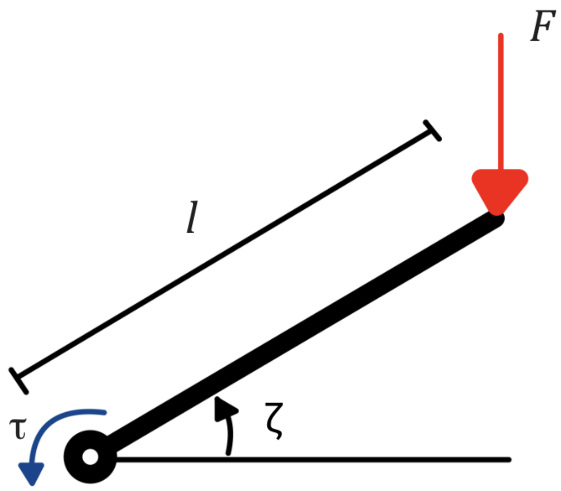

Figure 22: Annotated diagram of revolute joint load

Prismatic joints: Similarly, prismatic joints must also support loads they encounter. However, due to a shorter lever arm, the motors have lower torque requirements to maintain and move the same load. This is illustrated in Figure 23.

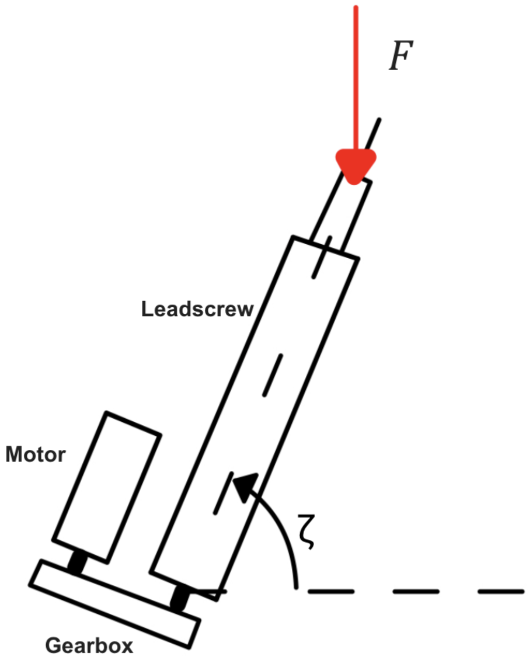

Figure 23: Annotated diagram of prismatic joint load

The torque required at the leadscrew of the linear actuator is:

$$M_L = F sin\phi \frac{L}{2\pi\eta} \tag{7}$$

where ϕ and F are defined in Figure 23, L is the axial distance travelled per revolution, and η is the mechanical efficiency of the leadscrew. For this calculation I set standard values for η and L at 0.35 and 5 mm, respectively. In the worst-case scenario (i.e. $\phi = 90°$), I get $\tau_p = 1.15\,\text{Nm}$.

It is worth noting that both of these mechanisms assume a 1:1 gear ratio between the motor and load. With a different assumed gear ratio, i, I get $\tau_{motor} = \frac{\tau}{i}$. In general, this calculation illustrates that I should take preference to mechanisms using linear actuators, to mechanisms with shorter link lengths, and to mechanisms that distribute the load on multiple kinematic chains.

Adjustment range estimate

While each architecture poses a different motion profile for height adjustment, there are two fundamental motions: prismatic and rotary. With a rotating mechanism (eg.

Folding, as drawn in Figure 24) z_{min} can almost reach 0. With just two 300 mm links the minimum range target can be achieved. For linear actuators, unless telescopic, the minimum length of the actuator must be at least half of the stroke length. This puts significant restrictions on z_{min} if the linear actuators are not configured creatively.

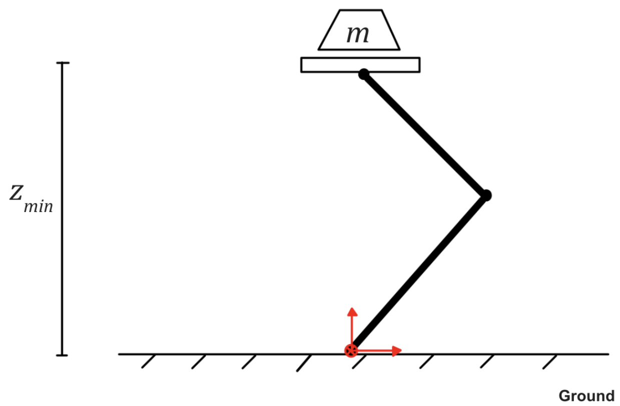

Figure 24: Annotated diagram of the adjustment range problem

Consequently, the adjustment range criteria favors folding mechanisms over extending links.

Actuation speed estimate

For linear actuators, I can approximate the vertical adjustment speed by reading the specifications of some industry grade products that match my requirements. Some of the fastest moving linear actuators could fulfill approximately 100 mm/s. To gain an estimate for the vertical position of a folding mechanism as a function of joint angles I can directly calculate the forward kinematics in two dimensions.

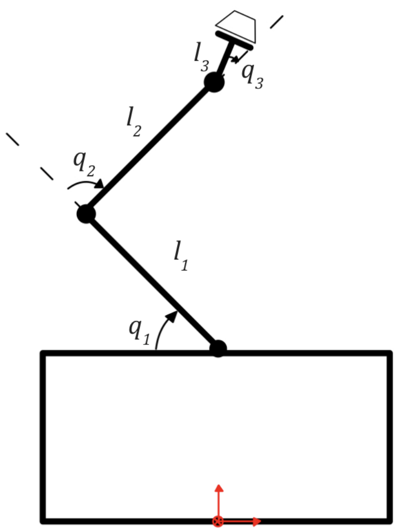

Figure 25: Annotated diagram of the adjustment speed calculation

The image illustrates the following equations:

$$z_* = l_1 sin(q_1) + l_2 sin(q_1 + q_2) \tag{8}$$
$$\dot{z}_* = l_1 \dot{q}_1 cos(q_1) + l_2(\dot{q}_1 + \dot{q}_2) cos(q_1 + q_2) \tag{9}$$

With the knowledge that the $\dot{q}_1$ and $\dot{q}_2$ are the angular frequencies of the motors w_1 and w_2, I can set some test values to determine the potential speed of elevation. With reasonable values for the angular frequency at $\dot{q}_1 = 90°/\text{sec}$ and $\dot{q}_2 = -90°/\text{sec}$ (with the link lengths both at 0.4 m and the starting angles in the flat position - i.e. $q_1 = 0°$, and $q_1 = 180°$). This gives a vertical elevation speed of approximately 628 mm/s, significantly above what I might be able to achieve with a linear actuator. It is worth noting that this velocity is dependent on the configuration and the torque on the motors will affect their maximum speed. However, these results suggest that folding mechanisms are preferred over linear mechanisms for this criteria.

Weight estimate

I performed a rough weight analysis of the components. For each architecture, I calculated the total weight by summing the individual components:

$$W_{total} = W_{links} + W_{joints} + W_{actuators} + W_{motors} + W_{electronics} + W_{auxiliary}$$

where:

W_{links} represents the summed weight of the links in the OnShape structural CAD (with material set to Aluminium 1060). W_{joints} represents the summed weight of the joints in the OnShape structural CAD (with material set to Stainless steel 300-series). $W_{actuators}$ is a fixed estimate on linear actuator weight to 3kg multiplied by the number of these actuators. W_{motors} is a fixed estimate on motor weight to 1kg multiplied by the number of these actuators. $W_{electronics}$ is a fixed weight of $500g$ across the board for circuits and wiring. Finally, I have $W_{auxiliary}$ for things like springs.

To facilitate direct comparison between different mechanisms, I normalized all weights by dividing by the minimum weight configuration, yielding dimensionless weight factors. This normalization allows me to quickly identify the relative weight penalty of choosing one mechanism over another, independent of absolute scale.

$$\text{Weight factor} = \frac{W_{\text{mechanism}}}{W_{\text{min}}}$$

Cost estimate

I performed a cost analysis for each architecture based on component pricing. My estimates were informed by market research for typical component costs:

$$C_{total} = C_{actuators} + C_{motors} + C_{auxiliary}$$

where: $C_{actuators}$ represents the cost of linear actuators at approximately €450 per unit multiplied by the number required ("SMAC Corporation Price Guide", 2023). C_{motors} represents the cost of motors at approximately €250 per unit multiplied by the number required (Transmission, 2024; "Hydroma Electric Motors Catalog", 2023). $C_{auxiliary}$ accounts for additional components such as springs ("Auxiliary Spring Applications", 2017).

I made the assumption that material and machining costs for the remaining parts would be approximately equal across all architectures as most components were either linear metal rods or 3D printed. Therefore, my comparative analysis focuses primarily on the relative costs of motors and off-the-shelf components, which constitute the most significant cost differentials.

To facilitate direct comparison between different mechanisms, I normalized all costs by dividing by the minimum cost configuration, yielding dimensionless cost factors.

This normalization allows me to quickly identify the relative cost penalty of choosing one mechanism over another, independent of absolute scale.

$$\text{Cost factor} = \frac{C_{\text{mechanism}}}{C_{\text{min}}}$$

10.3 Heuristics

In combination with the estimate calculations, several criteria could only be scored using heuristic estimates. This section covers each heuristic scoring approach along with attribution for validity.

Robustness

For robustness, I selected three heuristics based on design discussions with PR, other robotics engineers, and external references.

Factor	**Preference**	**Notes**
Actuator type	Linear > motors & linkages	Integrated and direct drive linear actuators are typically more robust due to fewer mechanical interfaces/failure points, higher rigidity, and simpler installation (Klemetson, 2020; Eitel et al., 2020).
Moving parts	Fewer > more	Fewer moving parts makes minimizes mechanical complexity, reduces the number of failure points, and lowers the risk of wear (Alpha Motor Corporation, 2020).
Mounting	Symmetric load paths > top-heavy and asymmetric	Symmetric load paths (eg. parallel) have more uniform load distribution and increased stability. Asymmetric load paths introduce stress concentrations and unpredictable responses which reduce robustness (Chen et al., 2022)

Table 5: Robustness heuristics

Noise level

It is desirable that the robot's elevation mechanism operates silently to reduce its interference with the on-board microphone in the robot.

Factor	Preference	Notes
Actuator type	Linear actuators with worm gears or lead screws > Stepper motors	Actuators with more mechanical contact points like gears and bearings are typically louder due to vibration and resonance. Integrated linear actuators tend to be quieter than stepper motors (Eaker and Mitra, 2020; Kimbell, 2019).
Drive mechanism	Direct drive or screw-driven > Belt drives > Chains or gear trains	Direct drive systems minimizes vibration through fewer mechanical interfaces. Screw-driven setups with well-lubricated contact points are also quiet (Taylor, 2025). In contrast, chain and gear trains are the loudest due to metal-on-metal contact and vibration, while belt drives offer a quieter alternative by absorbing motor noise and reducing vibration.

Table 6: Noise level heuristics

Portability

As the PR team and researchers often travel to various events like robotics conferences, portability is a key issue in their design philosophy. The following heuristics were used to evaluate it.

Factor	Preference	Notes
Collapsed size	Foldable and compact > bulky and rigid	When made smaller the mechanisms can be packaged neatly for transportation.
Tool-less disassembly	Quick-release and thumbscrews > Custom tools and finicky fasteners	PR engineers prefer that simple tools are used for disassembly and that fasteners are easily accessible.
Modularity	Broken into smaller parts > one big piece	PR engineers prefer separating the robot into typically three parts; torso, legs, and base.

Table 7: Portability heuristics

Repairability

Ensuring the robot is designed to be easily repaired by standard tools and techniques if it breaks down is an important part of research-focused robotics projects like Reachy. This means that customers can test and break components without being concerned for a hefty cost or long and complicated reparation periods.

Factor	**Preference**	**Notes**
Tools	Common tools like hex keys or screwdrivers > custom tools or machining	Commonly accessible tools in workshops or robotics research labs should ideally be usable on Reachy. 3D printing is preferred for broken components.
Standard parts	Off-the-shelf > custom	PR prefers either 3D-printable custom parts or motors and fasteners that can easily be replaced.
Accessibility	Components easy to reach > parts buried deep in an assembly	PR engineers have stated that they prefer easily accessible components and fasteners without packing and encumbering.

Table 8: Maintainability Factor Preferences and Considerations